A novel role for *dpp* in the shaping of bivalve shells revealed in a conserved molluscan developmental progaram

Koryu Kin, Shota Kakoi, Hiroshi Wada*

Graduate School of Life and Environmental Sciences, University of Tsukuba, 1-1-1 Ten-noudai, Tsukuba, Ibaraki 305-8572 Japan

Molecular and developmental basis for bivalve shell formation

Author for correspondence: Hiroshi Wada

Graduate School of Life and Environmental Sciences, University of Tsukuba, Tsukuba 305-8572 Japan

E-mail: hwada@biol.tsukuba.ac.jp

Tel & Fax: +81 29 853 4671

Abstract

During the molluscan evolution leading to the bivalves, the single dorsal shell was doubled. To elucidate the molecular developmental basis underlying this prominent morphological transition, we described the cell cleavage and expression patterns of three genes, *brachyury*, *engrailed*, and *dpp* in the Japanese spiny oyster *Saccostrea kegaki,* and examined the function of *dpp* in this species. The cleavage pattern of the *S. kegaki* embryo was nearly the same as the previously described pattern of other bivalve species, suggesting that the pattern itself is highly important for the establishment or the maintenance of the bivalve body plan. The expression pattern of a *brachyury* homolog in *S. kegaki* (*SkBra*) was similar to the pattern in gastopods even at the single cell level despite the deep divergence of gastropods and bivalves. *Engrailed* and *dpp* were previously found to be expressed around the shell anlagen in gastropods. Like that of gastropods, an *engrailed* homolog in *S. kegaki* (*SkEn*) was found to be expressed around the shell anlagen. However, the *dpp* homolog in *S. kegaki* (*SkDpp*) was expressed only in the cells along the dorsal midline. ZfBMP4 treatment experiments revealed the importance of *dpp* in establishing the characteristic shape of the bivalve shell anlagen.

Keywords: Bivalve; Mollusc; Shell; *Saccostrea kegaki*; Cell cleavage pattern; *Dpp*; *Engrailed*; *Brachyury*

Introduction

Although molluscan phylogeny is a matter of continued debate (Giribet et al., 2006; Lindberg et al., 2004), bivalves are generally thought to have evolved from a monoplacophoran-like ancestor having a single dorsal shell (Waller, 1998). The most prominent morphological change occurred during bivalve evolution is arguably the change in the number of shells, from univalvular to bivalvular. The change in shape must have been accompanied by changes in developmental processes and the underlying system that creates them. What kind of developmental changes led to the emergence of the bivalve shell is thus of considerable interest from an evolutionary, as well as a developmental perspective. Considering the widespread tinkering nature of developmental evolution (Carroll et al., 2005; Jacob, 1977; Wilkins, 2002), it is natural to assume that most of the developmental system for building a bivalve shell was employed conservatively from the developmental system for building a single dorsal shell. Some innovative changes were probably added later and, together with the formerly single-shell-forming system, constitute the bivalve-shell-forming system. Therefore, the first step toward elucidating this developmental evolution would be to determine which parts of the bivalve developmental system were present in the ancestral system and which are truly innovative components. This requires comparing bivalves to organisms that share the ancestral, single-shell-forming system, such as gastropods. In comparison to gastropods, bivalve embryogenesis has two notable features that seem to be intimately related to the formation of the bivalve shell. One is a feature in the cleavage pattern, and the other is a feature in the formation of the shell anlagen.

Both bivalves and gastropods develop by means of a “spiral cleavage” pattern [for details on spiral cleavage-based development, see, (Gilbert and Raunio, 1997; Henry and Martindale, 1999)]. In these embryos, the first two divisions generate four blastomeres, designated A, B, C, and D, which usually correspond to the left, ventral, right, and dorsal side of the future larval body (Fig. 1A, B). These blastomeres divide unequally to generate a quartet of micromeres on the animal tier, which are

designated by lowercase letters (e.g., 2d, $1a^2$; Fig. 1C). A micromere is not situated directly above its sister macromere because the orientation of the spindle is oblique with respect to the animal-vegetal axis. After the generation of the first quartet of micromeres, the macromeres continue to divide unequally to generate successive generations of animal micromere quartets. Thus, the largest cell in a spiral-cleaving embryo is usually one of the vegetal-most macromeres (Fig. 1D).

In bivalve embryos, after the second round of micromere generation, the largest cell is not one of the macromeres, but the 2d cell, which is one of the daughter cells of the 1D macromere (Fig. 1E). The 2d cell subsequently divides unequally four times, each time alternating the orientation and the relative position of the mitotic spindle in the cell. This pattern has been reported in detail for at least two bivalve species (Lilie, 1895; Meisenheimer, 1901), but not in gastropods or other molluscan species. Interestingly, the 2d cell was claimed to be the founder cell of bivalve shells (Lilie, 1895; Meisenheimer, 1901). Also, the first cell that divides bilaterally is the largest descendant of the 2d cell (Fig. 1F), not the 4d cell as in many gastropods. Given the importance of the 2d cell and its descendants in the bivalve embryo, a special notation was devised, in which the 2d cell and the largest descendant of the 2d cell are denoted as X until the bilateral cleavage stage. The first micromere generated from the X blastomere is X^1, the second is X^2, and so on.

Unfortunately, there have been virtually no detailed descriptions of cell cleavage patterns or cell lineage studies in bivalve embryos since the above-mentioned studies were conducted over a hundred years ago. Thus, we first examined the cell cleavage pattern of the embryos of the oyster *Saccostrea kegaki*, using fluorescent staining of cell boundaries and observation with a confocal laser scanning microscope (CLSM).

An understanding of cleavage patterns enabled us to determine the identity of blastomeres and to compare the lineage of specific gene expression cells between bivalve embryos and gastropod embryos. To examine the extent to which the global pattern of bivalve embryogenesis is comparable to that of

gastropods, we examined the expression pattern of the gene *brachyury*. The reasons for choosing *brachyury* were two-fold: first, the *brachyury* expression pattern was examined in detail in the gastropod *Patella vulgata* (Lartillot et al., 2002), to the extent that the identities of the cells expressing *brachyury* in the early embryos were determined; second, the *brachyury* expression pattern in blastomere formation seems to have been conserved among many animal groups (Arendt et al., 2001; Technau, 2001). Comparing cell identities is important, because the differences in the cleavage patterns of bivalves and gastropods might also be related to large differences in overall developmental patterning.

We also focused on the differences in the process of shell anlagen formation. The molluscan shell anlagen are usually called the "shell field" (Kniprath, 1981), a term we use here. We will briefly describe below the process of shell field formation in bivalves, which can roughly be divided into five phases: 1) establishment of the shell-founder cell, X, 2) expansion of X descendant cells on the dorsal surface, 3) invagination of the shell field, 4) evagination of the shell field and its successive expansion to cover a whole embryo, and 5) secretion of shell matrices and calcification in the shell field.

As we noted above, the shell field is derived mainly from the founder blastomere X, which continues to divide rapidly (phase 1). After the bilateral division of X, gastrulation begins at the vegetal pole of the embryo; the archenteron is derived from the vegetal macromeres. At the time when gastrulation begins, the descendants of X cover the dorsal surface of the embryo (phase 2, Fig. 1G, H). Then these X descendant cells invaginate, and the dorsal invagination called "shell filed invagination" (SFI) (Eyster and Morse, 1984), which represents the prospective shell field, appear (phase 3, Fig1I, J). The SFI of bivalves is not double but single, as in gastropods. After invagination, the SFI evaginates, and the shell field, which can be morphologically distinguished from surrounding cells in terms of cell height or the apparent demarcation between them, emerges onto the surface. The shell field then continues to expand laterally until it covers the whole embryo (phase 4, Fig. 1K, L). As the shell field

is covering the embryo, the secretion of shell matrix and calcification in the shell field begin and continue thereafter (phase 5).

Note that while the shell field of gastropods is circular, reflecting the shape of the SFI, the shell field in bivalves is dumbbell-shaped in which a constriction along the dorsal midline is apparent (Fig 6C-F). The constriction will develop into the hinge structure, which is a bivalve specific structure and enables their shells to open and close. We think that the formation of the hinge structure is critical in establishing a functional bivalve shell and believe that elucidation of the molecular mechanisms underlying its formation is especially important in understanding the evolution of the bivalve body plan.

Based on its expression patterns, the gene *engrailed* was suggested to have some function in shell development in gastropods and other mollusks (Moshel et al., 1998; Jacobs et al., 2000). In particular, *engrailed* is expressed around the shell field in the gastropod *P. vulgata* (Nederbragt et al., 2002). Also in *P. vulgata*, the gene *dpp* is expressed around a circular domain that is adjacent to the *engrailed* expression domain. Similar *dpp* expression was recently reported in another gastropod, *Haliotis asinina* (Koop et al., 2007). We isolated homologs of these genes in *S. kegaki* and examined their expression patterns in order to understand the development and evolution of the bivalve-specific shell structure. In the course of our study, we found that a *dpp* homolog in *S. kegaki* has a particularly interesting expression pattern with respect to the development of the hinge structure. To elucidate the function of *dpp* in *S. kegaki*, we used ZfBMP4, a homolog of *dpp* in the zebrafish. The results from functional assays suggest that a *dpp* homolog restricts expansion of the shell field on the dorsal midline.

Materials and Methods

Fertilization and embryo rearing

Adult oysters (*Saccostrea kegaki*) were collected at the coast near the Seto Marine Biological Laboratory, Kyoto University, Wakayama, Japan, and around the Shimoda Marine Research Center, University of Tsukuba, Shizuoka, Japan. Mature gametes were obtained by dissection and treated with 1 μM serotonin (serotonin-creatinine sulfate complex [Sigma] dissolved in filtered sea water [FSW]) to promote egg maturation. Embryos were fertilized with dissected sperm and cultured in FSW at 27°C. Proper density of the larvae in seawater is critical for the normal development of swimming gastrula into D-shaped larvae. We usually transferred swimming gastrula, about 6 h after fertilization, into fresh FSW to a density of less than 100 larvae/ml.

Fluorescent staining and observation with CLSM

Saccostrea kegaki embryos were stained with YOYO-1 fluorescent dye (Invitrogen) to visualize chromosomes, and with rhodamine-phalloidin (Invitrogen) to visualize cell boundaries. Prior to staining, embryos were treated with 1 mg/ml RNase in phosphate-buffered saline (PBS) at 37°C for 2 hours, in order to exclude cytoplasmic RNAs. Embryos were then stained with 10 units/ml rhodamine-phalloidin in PBT [PBS + 0.1% Tween-20] for about 1 hour at room temperature, followed by staining with 1 μM YOYO-1 in PBT for 5 minutes at room temperature. Embryos were subsequently washed three times with PBS and mounted in ~50% glycerol for observation. Optical sectioning images in the Z-axis were obtained with a Zeiss LSM510 confocal laser scanning microscope. 3D projection images

were reconstructed from Z-series images using a Zeiss LSM Image Browser (Carl Zeiss). Projected images were traced onto paper by hand, and individual blastomeres were then identified.

Cloning and phylogenetic analysis of SkBra, SkEn, and SkDpp

Partial fragments of *SkBra, SkEn,* and *SkDpp* were cloned by degenerate PCR using the following primers; *SkBra*: forward primer (5'- GTNAAYGGNGANTGGGTNCCNGG-3') and reverse primer (5'-AAYTTYTTNGCRAANGGRTTRTR-3'), *SkEn*: forward primer (5'-AARMGNCCNMGNACNGCNTTY-3') and reverse primer (5'-AAYTGRAACCANATYTTNAYYTG-3'), and *SkDpp*: forward primer (5'-GGNTGGRAYGAYTGGATHK-3') and reverse primer (5'-CCRCANCCNWCNACNACCAT-3'). The full coding sequences of *SkBra* and *SkDpp* were obtained by screening the cDNA library of gastrula embryos (Oda et al., 2002) using the Alkphos Direct Labeling and Detection System (Amersham). The longer cDNA fragment of *SkEn* was obtained by rapid amplification of cDNA ends (RACE) PCR using the BD SMART RACE cDNA amplification kit (Clontech) according to the manufacturer's instructions. The following primers were used for the RACE PCR: forward primer (5'-ATGGATTCCAAACAAGGACGTGATCCAGT-3') and reverse primer (5'-ACCTTCGTCTGACAGAGTGACGGTGGA-3'). The full sequence of each homolog was deposited in the DDBJ data bank (accession numbers, *SkBra*: AB379967; *SkDpp*: AB379969; *SkBMP5-8*: AB379970; and *SkEn*: AB379968).

Molecular phylogenetic analyses were performed as follows: Related sequences were retrieved from public databases based on BLAST searches and prior knowledge. Multiple alignments of related amino acid sequences were created using MUSCLE (Edgar, 2004), which were subsequently confirmed and modified manually, with unreliable regions trimmed. Phylogeny reconstruction was performed by

both maximum likelihood method using RaxML 7.0.4 (Stamatakis, 2006) and bayesian method using MrBayes 3.1.2 (Ronquist and Huelsenbeck 2003). Amino acid evolutionary models were selected using Prottest (Abascal et al., 2005). Specific models and options chosen are described in the legends of Supplementary figures 2, 3 and 4.

In situ hybridization

Digoxigenin (DIG)-labeled RNA probes were synthesized in vitro from the cDNA clones using the DIG RNA labeling kit (Roche). The embryos were fixed in a solution containing 4% paraformaldehyde, 0.1 M MOPS (pH 7.5), 2 mM EGTA, and 0.5 M NaCl, and stored in 80% ethanol at –20°C. In situ hybridization was performed following the protocol for ascidian embryos (Yasuo and Satoh, 1994), except that the RNase treatment was omitted during the washing process. Briefly, after rehydration the embryos were treated with 2 μg/ml Proteinase K at 37°C for 20 min and then post-fixed in 4% paraformaldehyde. After prehybridization, the embryos were hybridized with digoxigenin-labeled probes at 55°C (hybridization buffer: 50% formamide, 6× SSC, 5× Denhart's solution, 100 μg/ml yeast RNA, and 0.1% Tween 20). Excess probes were removed by washing the embryos twice in 50% formamide, 4× SSC, and 0.1% Tween 20, twice in 50% formamide, 2× SSC, and 0.1% Tween 20, and twice in 50% formamide, 1× SSC, and 0.1% Tween 20. The embryos were then incubated with 0.5% blocking reagent in PBT for 30 minutes at room temperature. After blocking, embryos were incubated with alkaline phosphate-conjugated anti-digoxigenin antibodies, and positive immunoreactions were visualized using Nitro blue tetrazolium/ 5-Bromo-4-chloro-3-indolyl phosphate (NBT/BCIP) solution (Roche).

In some cases, we performed double-staining experiments to confirm the orientation of an early stage embryo. For double staining, embryos were simultaneously hybridized with fluorescein-labeled

probes of *Sk-β-tublin* (Kakoi et al., 2008), along with digoxigenin-labeled probes. After embryos were visualized for the digoxigenin-labeled probe, following the steps described above, embryos were incubated with 0.1M glycine-HCl (pH 2.2) for 30 minutes at room temperature. After post-fixation with 4% paraformaldehyde, the blocking and visualization steps were performed as described above, except that we used alkaline phosphate-conjugated anti-fluorescein antibodies instead of the anti-digoxigenin antibodies, and we used Fast Red (Sigma) for visualization.

BMP4 treatment experiments

Recombinant zebrafish (Zf) BMP-4 (R&D Systems) was dissolved into 0.1% bovine serum albumin (BSA) in PBS to make up 1 μM stock solution. Embryos were incubated at 27°C in 10 nM, 20 nM, 40 nM, or 80 nM Zf-BMP4 from 3 hours post fertilization (hpf) until 12.5 hpf, when they were fixed for in situ hybridization. Control embryos were incubated at 27°C during the same developmental time period in 10 μl 0.1% BSA in PBS/ ml, 20 μl/ml, 40 μl/ml, and 80 μl/ml FSW corresponding to the 10 nM, 20 nM, 40 nM, and 80 nM Zf-BMP4 treatments, respectively. Both Zf-BMP4 treated and control embryos were transferred into fresh solution containing corresponding concentrations of reagents at about 6 hpf at a density of less than 100 embryos/ml. The boundary of the shell field was visualized by in situ hybridization using the *SkEn* probe. Images of embryos were captured with a Nikon DXM1200 digital camera attached to a Nikon ECLIPSE E800 microscope, and measurements were obtained using the image processing program ImageJ (Abramoff et al., 2004). Statistical analyses were carried out using R 2.6.0 (Ihaka and Gentleman, 1996).

Results

Cleavage patterns of the Saccostrea kegaki embryo

Cell boundaries of early *S. kegaki* embryos were visualized by staining with rhodamine-phalloidin, which binds to actin filaments backing the cell membrane (Fig. 2A). Embryos were simultaneously stained with YOYO-1, which binds to nucleic acids to visualize chromosomes (Fig. 2B). Chromosome visualization enabled us to distinguish mitotic-phase chromosomes from gap-phase chromosomes, thus helping us to determine the order of cell cleavage. We traced cell outlines of the 3D projected embryo images by hand from different angles, in succession, from the 8-cell stage to the 49-cell stage (Fig. 3, 4). We then determined the identities of individual blastomeres by comparing each drawing and following the conventional spiralian blastomere nomenclature (Conklin, 1897; Fig. 2C-F, 3, 4). Using this method, we obtained a diagram showing the order of cell cleavage (Fig. 2G). Some ambiguities concerning the order of cell cleavage remain because we did not observe all of the individual cell cleavage stages leading to the 49-cell stage. Furthermore, in some cases, cell division occurs in a different order in different embryos. For example, at about the 20-cell stage, $1b^2$ divided earlier than $1c^2$ in one embryo, whereas the latter divided earlier than the former in another embryo (Supplementary Fig. 1). When we could not confidently determine the order of cell cleavage, we indicated this in the diagram as a simultaneous division.

The cleavage pattern of *S. kegaki* embryo was almost the same as previously described in other bivalve embryos (*Unio*: Lilie, 1895; *Dreissena*: Meisenheimer, 1901). We will briefly explain below the early cleavage pattern of *S. kegaki* embryo with special reference to the cleavage pattern of the blastomere X. After the first micromere generation (Fig. 3A, B), the 1D macromere generates the larger "micromere" X, or 2d, and the smaller macromere 2D to reach the 9-cell stage embryo (Fig. 1E). The other micromeres and macromeres then generate the second generation of blastomeres to reach 16-cell stage embryo. The 17-th blastomere is X^1, or $2d^2$, which is the first descendant of the blastomere X,

budded to the vegetal-right side of X (Fig. 3C, D). The blastomere X successively generate X^2, the second descendant of X, to the vegetal left side, meanwhile 2D and the $1q^2$ ($1a^2$-$1d^2$) divide to generate the third generation blastomeres (Fig. 3E, F). Then the first descendant of X, X^1, divides to reach the 24-cell stage. The 28-cell stage is reached by the division of 2a-2c and X. This third division of X is different from previous ones in that it buds X^3 to the animal-central side of it (Fig. 4A, B). Before the fourth X division, $1q^1$($1a^1$-$1d^1$), 2A-2C, and the 3D blastomeres divide. The division of 3D is particularly notable because this division generates the mesoblast M, or 4d. Then X buds the fourth descendant, this time again changing direction to the vegetal-central side of it (Fig. 4C, D). Almost at the same time, the $1q^2$ lineage cells ($1a^{21}$-$1d^{21}$ and $1a^{22}$-$1b^{22}$), which are called "trochoblasts" because they will contribute to the prototroch of larva, divide and the quartet of trochoblasts can be seen for each quadrant. Meanwhile, X divide bilaterally for the first time (Fig. 4E, F). Following the bilateral division of X, the mesoblast M also divides bilaterally (Fig. 4E, F). The embryo begins to transform from spiral to bilateral symmetry after these bilateral cell divisions.

Saccostrea kegaki *homologs of* brachyury*,* dpp*, and* engrailed

SkBra encodes 450 amino acids, the T domain of which is 89% identical to the *brachyury* homolog of *P. vulgata* (Nederbragt et al., 2002). Molecular phylogenetic analysis using the T domain revealed that *SkBra* formed a monophyletic clade with *brachyury* homologs of other species (Supplementary Fig. 2).

SkEn encodes 229 amino acids and contained all of the five conserved domains found in the *engrailed* homologs from other species (data not shown). Molecular phylogenetic analysis using the homeodomain also showed that *SkEn* formed a monophyletic clade with *engrailed* homologs of other species (Supplementary Fig. 3).

SkDpp encodes 421 amino acids, and the TGF-beta domain was 99% identical to *mGDF1*, which is a *BMP2/4* ortholog, in the oyster *Crassostrea gigas* (Herpin et al., 2004; Lelong et al., 2000). In the course of isolating *SkDpp*, we obtained another cDNA clone, which was a presumed homolog of the BMP family of genes, whose amino acid sequence was 89% identical to *GDF4*, a *BMP5-8* homolog, in *C. gigas* (Herpin et al., 2004). Thus we designated this clone *SkBMP5-8*, and analyzed the molecular phylogenetic relationships between *SkDpp* and other BMP related genes including *SkBMP5-8*. As predicted, *SkDpp* formed a monophyletic group with the *BMP2/4* homologs of other species, and *SkBMP5-8* with the *BMP5-8* homologs (Supplementary Fig. 4).

Expression of SkBra

SkBra expression was first detected in embryos at about the 16-cell stage. No maternal expression was detected. The blastomere first expressing *SkBra* was identified as 2D. The 2D blastomere soon divided and *SkBra* expression was inherited in one of the daughter cells, 3d. Shortly thereafter, additional expression was detected in the blastomere identified as $2d^{22}$ (X^{12}) and 3c (Fig. 5A-D). These cells precisely correspond to the cells in which expression of a *brachyury* homolog (*PvuBra*) was reported in *Patella vulgata* embryos (Lartillot et al., 2002), although slight differences in early expression pattern exist between the two genera. In *Patella* embryos, the first indication of *PvuBra* expression was detected in the 3D blastomere, whereas it was first seen in 2D in *Saccostrea* embryos. Also, in *Patella* embryos, weaker expression of *PvuBra* was reported in cells other than the above-mentioned blastomeres, while we did not detect such expression in other blastomeres in *Saccostrea* embryos. However, even in *P. vulgata* embryos, this weaker expression pattern soon disappeared and *PvuBra* expression was later restricted to 3c, 3d, and $2d^2$ derivatives.

SkBra expression was subsequently detected in the cells located in the vegetal region where the descendant cells of 3d, $2d^{22}$ and 3c presumably resided, but we could not determine the identities of

those cells due to the lack of a cell arrangement map up to this stage. *SkBra* expression persisted and propagated in the ventral to vegetally-dorsal region (Fig. 5E-J). The ventral expression pattern of *SkBra* is reminiscent of that of *Patella* (Lartillot et al., 2002), in which *PvuBra* is expressed along the ventral midline. However, the expression domain of *SkBra* is more laterally expanded compared to *PvuBra*. The ventral-anteriormost domain of *SkBra* expression is not just beneath the blastopore, as there are always one or more cells intervening between the *SkBra* expression domain and the blastopore (Fig.5I). The dorsal-anteriormost extent of *SkBra* expression is several cells below the SFI. After the shell field evaginates, the *SkBra* expression domain shrinks and becomes restricted to the prospective anus, and eventually disappears in the late larval stage (data not shown).

Expression of SkEn

SkEn expression was only detected in the swimming-larval-stage of embryos, and there was no detectable expression in the early cleavage stage. In the shell field invagination stage, *SkEn* expression was detected around the entrance of the SFI (Fig. 6A, B). After the shell field evaginated, expression of *SkEn* was detected around the evaginated shell field. Thus, a dumbbell-shaped expression domain was observed (Fig. 6C, D). *SkEn* expression was also detected, albeit much fainter than in the borderline cells, in the rest of the shell field cells. *SkEn* expression persisted around the shell field during the development of the larva into the D-shape.

Note that in contrast to the previous claim of bivalve *engrailed* expression (Jacobs, 2000), a distinct strong expression domain along the hinge region was not detected. Expression of *SkEn* in the hinge region was at the same level as the weak expression in the non-border cells of the shell field during “phase 4”, i.e. before calcification and secretion of shell matrices in the shell field (Fig. 6C E). At “phase 5” reproducible strong staining with a *SkEn* probe began to be detected in the hinge region. However, it is likely that this was a result of unspecific staining, since the sense probe, as well as the

anti-sense probe, of *SkEn* stained the hinge region in phase 5 (Fig. 6G; Kakoi et al. 2008). This nonspecific staining was easily distinguished from a true signal because the former was always observed on the surface or outside of the cell bodies, whereas the latter was uniformly observed in the cytoplasm (Fig. 6G).

Expression of SkDpp

SkDpp expression was first detected in the $2d^2$ (X^1) blastomere at about the 18-cell stage. No maternal expression was detected. Subsequently, the $2d^2$ blastomere divided and *SkDpp* expression persisted in one of the daughter cells. Soon after the X blastomere divided bilaterally, additional *SkDpp* expression began to be detected in the $1d^{12}$ blastomere (Fig. 7A,B). *SkDpp* expression persisted in two cells, which were probably the descendants of the $2d^2$ and $1d^{12}$ blastomeres. After the commencement of shell field invagination and gastrulation, *SkDpp* expression seemed to be restricted to one cell anterior to the SFI, presumably a $1d^{12}$ derivative, and one cell posterior to the SFI, presumably a $2d^2$ derivative (Fig. 7C). At the stage when the shell field completely invaginated, the cells expressing *SkDpp* lay just anterior and posterior to the SFI (Fig. 7E, G).

After shell field evagination, *SkDpp* expression was detected in the hinge region (Fig. 7J, K). Given that the *SkDpp*-positive cells had been located above and beneath, i.e., outside of, the shell field, the *SkDpp* expression domain topologically shifted between the shell field invagination and evagination stages. This shift may have been a result of the transition of *SkDpp* expression to different cells or a result of the movement of *SkDpp*-positive cells. We suggest that the latter is the case for two reasons. Firstly, there were embryos in which *SkDpp* expression was detected in the cells adjacent to the shell field shortly after shell field evagination (Fig. 7I). This means that the shift of *SkDpp* expression to the hinge region after shell field evagination occurred in a fairly short time span. Secondly, if a transition of expression to different cells occurred, there should be embryos with stained cells both outside the

shell field and in the hinge region, representing a transitional phase. However, we never found such embryos. Thus we think it is more likely that *SkDpp*-positive cells migrate into the hinge region from outside the shell field, although we cannot be certain without further experiments such as cell labeling. After the larvae became D-shaped, *SkDpp* expression was no longer detected.

Zebrafish BMP4 treatment reduced the size of the shell field

Herpin et al. (2005) reported that an oyster BMP receptor could transduce BMP signaling in a zebrafish embryo. This in turn suggests that zebrafish BMP can be a ligand for an oyster BMP receptor and drive downstream signaling cascades. Indeed, zebrafish BMP can activate specific signaling cascades in other invertebrates, such as amphioxus or hemichordates (Lowe et al., 2006; Yu et al., 2007). We therefore used ZfBMP4, a zebrafish homolog of *SkDpp*, in the hope of reinforcing dpp signaling. We exposed *S. kegaki* embryos to different concentrations of ZfBMP4 and examined the effects by visualization of the shell field using whole mount *in situ* hybridization staining of *SkEn*.

Even at the highest concentration tested (80 nM), the expression domain of *SkEn* always encircled the dorsal region of an embryo and did not become patchy or diminished. This suggests that the specification of *engrailed*-positive cells, namely the boundary cells of the shell filed, is independent of dpp signaling. However, the shape of the *SkEn* encircling domain is apparently different between the treated and control embryos (compare Fig. 8E to 8H).

To quantitatively confirm the change in shape, we measured the embryo along three lengths: the embryo length, the central length of the *SkEn*-encircling domain, and the lateral length of the domain (Fig. 8A). We examined whether ZfBMP4 affected the general growth of an embryo by comparing the length of embryos between the treated and control groups (measurements are summarized in Supplementary Table 1). Significant differences were not detected in embryo length, suggesting that ZfBMP4 did not generally adversely affect bivalve embryogenesis (Supplementary Fig. 5). Significant

differences in the central length of the *SkEn*-positive domain were detected in most treatments, except in the case of the 40 nM treatments (Fig. 8B). The lateral length of the *SkEn*-positive domain was severely reduced in all treatments (Fig. 8C). To determine the relative extent to which the lateral and central lengths of the embryo were affected, we also examined the effect of ZfBMP4 on the ratio of the lateral length to the central length of the embryo (Fig. 8D). Treatment with ZfBMP4 above 10 nM reduced the ratio of the lateral length to the central length, indicating that the lateral length was affected more severely by the treatment, thus causing a change in the shell field shape (Fig. 8E-J).

There are at least two possible explanations for the reductive effects of ZfBMP4 on lateral length; the reduction of the lateral length might be caused by the reduction in the size of the cells in the lateral region, or it might be caused by the reduction in the number of cells in the lateral region. Although we cannot conclude whether either scenario is the case without accurately counting the number of shell field cells, we note that nuclear staining of embryos showed that the latter explanation seemed more likely (compare Fig. 8F to 8I). The number of cells in the *SkEn*-positive domain of ZfBMP4-treated embryos apparently decreased compared to the controls, whereas the size of the cells did not seem to be affected.

Discussion

Conservation of blastomere identity between gastropods and bivalves

The cleavage pattern of the *S. kegaki* embryo, including the characteristic cleavage pattern of blastomere X, was almost the same as the previously described pattern of bivalve embryos (*Unio*: Lilie, 1895; *Dreissena*: Meisenheimer, 1901). The bivalve species used in those studies and ours are not phylogenetically close. Taxonomically, *Unio* belongs to the order Unionoidae, *Dreissena* to the order Pteroida, and *Saccostrea* to the order Ostreoida. According to the scheme based on the combined morphological and molecular data in a recent phylogenetic analysis (Giribet and Wheeler, 2002), the phylogenetic group that includes the above three species is Autolamellibranchia, which includes most of the bivalve mollusks, except for the Protobranchia. It is therefore probable that the stereotypic cleavage pattern of the bivalve embryos described in the above three species is shared among other bivalve species. The remarkable conservation of the cleavage pattern in bivalves suggests that the cleavage pattern itself is important for the establishment, or the maintenance, of the bivalve body plan phylogenetically, as well as ontogenetically.

It was possible to identify an individual blastomere expressing a specific gene only after establishing a cell arrangement map for the *S. kegaki* embryo. With the aid of the map, we examined the *SkBra* expression pattern in detail. Surprisingly, the blastomeres, which expressed *SkBra*, corresponded to the blastomeres that expressed *brachyury* in *P. vulgata* embryos. This indicates that "blastomere identity" is conserved despite the deep divergence and drastic differences in cleavage patterns between the two species.

SkEn expression and the nature of the bivalve condition

Engrailed homologs have been shown to be related in shell field formation in various molluscan species (Polyplacophora: Jacobs et al., 2000; Scaphopoda: Wanninger and Haszprunar, 2001; Gastropods: Moshel et al., 1998; Nederbragt et al., 2002; Iijima et al., 2008; Cephalopoda: Baratte et al., 2007; Shigeno et al., 2008). Only one study to date has been reported for bivalves. In that study, Jacobs et al. (2000) reported on the expression pattern of an *engrailed* homolog in the embryo of the clam *Transennella tantilla*. They detected *engrailed* homolog expression along the hinge, as well as around each developing valve in the clam, using a 231-bp probe containing the homeodomain. Their study suggested that the expression of engrailed along the hinge provided evidence for a unique bivalve condition in shell field formation.

In our study, we detected strong *SkEn* expression around the dumbbell-shaped shell field, confirming the conserved role of *engrailed* in shell field formation in various mollusks. However, we found that along the hinge line, *SkEn* expression was at the same level as the weak expression of surrounding shell field cells during "phase 4". During this phase, a strong expression domain was detected around the dumbbell-shaped shell field as a whole. At "phase 5", the stage in which calcification of the hinge region and the shell field as a whole commences, strong staining along the hinge was also observed. However, this staining was apparently nonspecific due to the absorbance of probes by calcified tissue; that is, similar staining was observed along the hinge region even when we used the sense probe instead of the antisense probe, and the staining was not observed inside the cytoplasm but on the surface or outside of the cell.

These observations do not necessarily mean that *SkEn* has no role in hinge "growth" at and after phase 5. Strong "true" underlying *SkEn* expression may have been masked by nonspecific staining. However, note that *SkEn* expression was much weaker than that in the edge, and at the same level as in the rest of the shell field in phase 4, which is a crucial step in establishing the hinge region. Therefore, we concluded that *SkEn* may not have a causal role in "establishing" the hinge structure.

The discrepancy in observed *engrailed* expression patterns between our study and that of Jacobs et al. (2000) might reflect molecular developmental differences used in establishing the hinge between the two species, or it may be due to artifacts. Regarding the latter point, note that the shell field in bivalves is particularly prone to nonspecific staining, probably due to calcification or secretion of shell matrices onto the surface. Even at phase 4, depending on the length of staining period or the concentration of probes, we sometimes found nonspecific staining around the hinge or other places in the shell field, although such staining was not reproducible (an example of such nonspecific staining shown in Fig. 6E and F). At phase 5, nonspecific staining along the hinge and around the shell field after a certain period of incubation was almost unavoidable using our current technique. With regard to the data of Jacobs et al. (2000), we cannot measure the possibility of artifacts because they provided no information about the developmental stage of the embryos used. Further examination of *engrailed* homolog expression patterns in other bivalve species will help clarify this issue.

Therefore, we think that the previously accepted role of *engrailed* in bivalve hinge formation should be reconsidered. Our results suggest that the bivalve shell field is seamless with respect to *engrailed* expression, and the hinge region is different from the margin of the shell field. These suggestions are consistent with the morphological knowledge in that the hinge ligament has been described to have a similar layer-structure as the rest of the shell (Owen et al., 1953; but see also Waller, 1998 for exceptions and other discussions). In other words, the hinge region represents "local modification" (Owen et al., 1953) of the shell valves rather than just the demarcation of two valves. As discussed below, the unique condition of the bivalve shell field may be better described as a local modification along the dorsal midline of a single *engrailed* bearing shell field through mechanisms such as *dpp* expression.

SkDpp expression and function: implications for the establishment of the hinge structure

The expression pattern of *dpp* has been reported in four gastropod species to date: *Ilyanassa obsoleta* (Lambert and Nagy, 2002), *Patella vulgata* (Nederbragt et al., 2002), *Haliotis asinina* (Koop et al., 2007), and *Lymnaea stagnalis* (Iijima et al., 2008). Early expression patterns were reported in *I. obsoleta* and *H. asinina* (Koop et al., 2007; Lambert and Nagy, 2002); there are some differences in the expression patterns of the two species, but basically, *dpp* is expressed symmetrically in micromeres (in *I. obsoleta*, the 3D macromere also expresses *dpp*) in the early cleavage stages. In later stages, *dpp* expression was found to surround the developing shell field (Nederbragt et al., 2002; Koop et al., 2007), or to mark the right-handed area of the invaginated shell field (Iijima et al., 2008). These *dpp* expression pattens in later stages suggest a *dpp* role in shell formation in gastropods, although this role has not been corroborated to date with functional assays.

The expression pattern of *SkDpp* differs significantly from that of the *dpp* homolog in gastropods. In the early cleavage stages, *SkDpp* was expressed asymmetrically at two sites in the dorsal micromeres, one above the X cells and another below. These two separate expression domains persisted until the shell field invagination stage, at which time the two expression domains clip the SFI on the dorsal midline. After evagination of the shell field, the two domains fuse in the hinge region, possibly due to the migration of *SkDpp*-positive cells.

The difference in *dpp* expression patterns between bivalves and gastropods is remarkable considering the seemingly conservative nature of gene expression patterns between gastropods and bivalves as revealed from the results of *brachyury* and *engrailed* (compare Fig. 9I and J to Fig. 9 E-H). The absence of expression around the shell field suggests that *SkDpp* is not involved in shell field formation in the bivalve embryo *per se*. Instead, hinge region expression suggests the involvement of *SkDpp* in establishing the hinge structure.

Due to the small size of the embryos, among other reasons, microinjection or electroporation in *S. kegaki* embryos is extremely difficult. The lack of gene-specific knockdown or knockout methods

led us to use a zebrafish homolog in order to investigate the function of dpp signaling pathways in *S. kegaki*. As suggested from the expression patterns of *SkDpp*, even a high concentration of ZfBMP4 on bivalve embryos did not diminish *engrailed* bearing cells on the dorsal side. That is, specification of the shell field cells was not affected by exposure to ZfBMP4. This indicates that *SkDpp* is not involved in the specification of the shell field cells. Instead, we found that the amount of ZfMP4 exposed was related to the size of the shell field: a high amount of ZfBMP4 decreased the size of the shell field, supposedly through the inhibition of the proliferation of the shell field cells. This suggests that *SkDpp* has a role in restricting the expansion of the shell field on the dorsal midline.

Neverthless, we would like to discuss some serious disadvantages of utilizing exogenous proteins from different species. Such disadvantages are that ZfBMP4 may not reinforce dpp signaling pathways in oyster embryos, or that ZfBMP4 may bind to other TGF-beta receptors and reveal phenotypic effects through such nonspecific binding. However, we argue that the first point is not the case because experiments using another oyster species (Herpin et al., 2005) showed that the oyster BMP receptor bound to zebrafish ligands and transduced signals downstream. As for the second point, we believe that if this had been the case, anomalies in other aspects of embryogenesis would have occurred. However, we only observed shell-field specific phenotypic effects. Furthermore, these shell-field related phenotypic effects are consistent with shell-field related expression patterns of *SkDpp*. Therefore, even if we had obserevd effects due to nonspecific ligand-receptor interactions, these effects could have been redundant to the effects through dpp signaling. Although more gene-specific methods such as RNAi or morpholino-antisense oligonucleotide base methods should be employed in order to determine the specific function of *Skdpp* in shell formation, we think it is appropriate to consider that the phenotypic effects of ZfBMP4 on the bivalve shell field are caused by reinforcing dpp signaling, thus revealing a *SkDpp* function.

Based on the results of the *SkDpp* expression pattern and the functional assays using ZfBMP4, we propose a hypothesis for the role of *SkDpp* in bivalve shell formation below. *SkDpp* is expressed in the anterior and the posterior cells to the shell founder cell, X, along the dorsal midline from a fairly early stage of embryogenesis (Fig. 9A, B). The topological relationship between the *SkDpp*-positive cells and the shell founder cells does not change until the shell field evagination stage, and the *SkDpp*-positive cells reside on the anterior and the posterior lip of the SFI in this stage (Fig. 9C). Dpp proteins may inhibit the proliferation of the shell field, which results in the reduction of shell field length, especially along the dorsal midline, generating the characteristic bivalve dumbbell-shaped shell field (Fig. 9E). Subsequently, the *SkDpp*-positive cells apparently migrate into the hinge region (Fig. 9G). The hinge region will become the ligament, a largely uncalcified structure (Owen et al., 1953) that enables a bivalve shell to open and close. Although there is still only indirect evidence for such cell migration, the migration of *SkDpp*-positive cells can be thus considered to be important because without it the hinge region would be covered by shell field cells, which secrete calcified shell matrix, and would be unmovable. “Local modification” along the dorsal midline in the shell field is needed to avoid such an unfavorable situation, and *SkDpp* and *SkDpp*-positive cells may have roles in modifying the dorsal midline of the shell field. The generation of such functions in the *dpp* and *dpp*-positive cells may have been critical in the evolutionary transition from univalves to bivalves. If our hypothesis is correct, ablation of the *SkDpp*-positive cells, or inhibition of dpp signaling, will result in a bivalve embryo with a single shell without a hinge structure. However, it is not known to what extent the *SkDpp*-positive cells actually contribute to hinge structure formation. Further elucidation of the function of *SkDpp* and the nature of *SkDpp*-positive cells will be the next challenge in uncovering the developmental mechanisms underlying one of the most prominent morphological transitions in molluscan evolution.

Acknowledgements

We thank Yasuko Oda-Akiyama and Hiroki Oda for providing the cDNA library of *S. kegaki*. We also thank the staffs of Seto Marine Biological Laboratory of Kyoto University and Shimoda Marine Research Center of University of Tsukuba, for their kind support in collecting specimens.

References

Abascal, F., Zardoya, R., Posada, D., 2005. ProtTest: Selection of best-fit models of protein evolution. Bioinformatics 21, 2104-2105.

Abramoff, M. D., Magelhaes, P. J., Ram, S. J., 2004. Image Processing with ImageJ. Biophoto. Internatl. 11, 36-42.

Arendt, D., Technau, U., Wittbrodt, J., 2001. Evolution of the bilaterian larval foregut. Nature 409, 81-5.

Baratte, S., Andouche, A., Bonnaud, L. 2007 *Engrailed* in cephalopods: a key gene related to the emergence of morphological novelties. Dev. Genes. Evol. 217, 353-62.

Carroll, S. B., Grenier, J. K., Weatherbee, S. D., 2005. From DNA to Diversity. Blackwell Publishing, Ltd., Malden.

Dan, K., Sekiguchi, K., Ando, Y., Watanabe, H., 1983. Invertebrate Embryology. Baifukan, Co., Ltd., Tokyo.

Eyster, L. S., Morse, M. P., 1984. Early Shell Formation During Molluscan Embryogenesis, with New Studies on the Surf Clam, *Spisula solidissima*. Amer. Zool. 24, 871-882.

Edgar, Robert C., 2004. MUSCLE: multiple sequence alignment with high accuracy and high throughput, Nuc. Acids Res. 32, 1792-97.Gilbert, S. F., Raunio, A. M. (Eds), 1997. Embryology: Constructing the Organism. Sinauer Associates, Inc., Sunderland.

Giribet, G., Okusu, A., Lindgren, A. R., Huff, S. W., Schrodl, M., Nishiguchi, M. K., 2006. Evidence for a clade composed of molluscs with serially repeated structures: monoplacophorans are related to chitons. Proc. Natl. Acad. Sci. USA 103, 7723-8.

Giribet, G., Wheeler, W., 2002. On bivalve phylogeny: a high-level analysis of the Bivalvia (Mollusca) based on combined morphology and DNA sequence data. Invert. Biol. 121, 271-324.

Henry, J. J., and Martindale, M. Q., 1999. Conservation and innovation of the spiralian development. Hydrobiol. 402, 255-265.

Herpin, A., Lelong, C., Becker, T., Rosa, F., Favrel, P., Cunningham, C. 2005. Structural and functional evidence for a singular repertoire of BMP receptor signal transducing proteins in the lophotrochozoan Crassostrea gigas suggests a shared ancestral BMP/activin pathway. FEBS J. 272, 3424-40.

Herpin, A., Lelong, C., Favrel,, P. 2004. Transforming growth factor-beta-related proteins: an ancestral and widespread superfamily of cytokines in metazoans. Dev. Comp. Immunol. 28, 461-85.

Ihaka, R., Gentleman, R., 1996. R: A Language for Data Analysis and Graphics. J. Comp. Graph. Stat. 5, 299-314.

Iijima, M., Takeuchi, T., Sarashina, I., Endo, K. 2008. Expression patterns of engrailed and dpp in the gastropod Lymnaea stagnalis. Dev. Genes. Evol. 2008. 218, 237-51.

Jacob, F., 1977. Evolution and tinkering. Science 196, 1161-6.

Jacobs, D. K., Wray, C. G., Wedeen, C. J., Kostiken, R., Desalle, R., Staton, J. L., Gates, R. D., Lindberg, D. R., 2000. Molluscan engrailed expression, serial organization, and shell evolution. Evol. Dev. 2, 340-347.

Kakoi, S., Kin, K., Miyazaki, K., Wada, H., 2008. Early development of the Japanese oyster (*Saccostrea kegaki*): Characterization of some genetic markers. Zool. Sci. 25, 455-464.

Kniprath, E., 1981. Ontogeny of the Molluscan Shell Field: a Review. Zool. Scr. 10, 61-79.

Koop, D., Richards, G. S., Wanninger, A., Gunter, H. M., Degnan, B. M., 2007. The role of MAPK signaling in patterning and establishing axial symmetry in the gastropod *Haliotis asinina*. Dev. Biol. 311, 200-12.

Lambert, J. D., Nagy, L. M., 2002. Asymmetric inheritance of centrosomally localized mRNAs during embryonic cleavages. Nature 420, 682-6.

Lartillot, N., Lespinet, O., Vervoort, M., Adoutte, A., 2002. Expression pattern of *Brachyury* in the mollusc Patella vulgata suggests a conserved role in the establishment of the AP axis in Bilateria. Development 129, 1411-21.

Lelong, C., Mathieu, M., Favrel, P., 2000. Structure and expression of mGDF, a new member of the transforming growth factor-beta superfamily in the bivalve mollusc *Crassostrea gigas*. Eur. J. Biochem. 267, 3986-93.

Lilie, F. R., 1895. The Embryology of the Unionidae. J. Morph. 10, 1-100.

Lindberg, D. R., Ponder, W. F., Haszprunar, G., 2004. The Mollusca: Relationship and Patterns from Their First Half-Billion Years. *In* "Assembling the Tree of Life" (J. Cracraft and M. J. Donoghue, Eds.), pp. 252-278. Oxford University Press, Inc., New York.

Lowe, C. J., Terasaki, M., Wu, M., Freeman, R. M., Jr., Runft, L., Kwan, K., Haigo, S., Aronowicz, J., Lander, E., Gruber, C., Smith, M., Kirschner, M., Gerhart, J., 2006. Dorsoventral patterning in hemichordates: insights into early chordate evolution. PLoS Biol. 4, e291.

Meisenheimer, J., 1901. Entwicklungsgeschichte von Dreissensia polymorpha Pall. Zeitschrift f. wissensch. Zoologie. 69, 1-137.

Moshel, S. M., Levine, M., Collier, J. R., 1998. Shell differentiation and engrailed expression in the *Ilyanassa* embryo. Dev. Genes. Evol. 208, 135-41.

Nederbragt, A. J., van Loon, A. E., Dictus, W. J., 2002. Expression of *Patella vulgata* orthologs of *engrailed* and *dpp-BMP2/4* in adjacent domains during molluscan shell development suggests a conserved compartment boundary mechanism. Dev. Biol. 246, 341-55.

Oda, H., Wada, H., Tagawa, K., Akiyama-Oda, Y., Satoh, N., Humphreys, T., Zhang, S., Tsukita, S., 2002. A novel amphioxus cadherin that localizes to epithelial adherens junctions has an unusual domain organization with implications for chordate phylogeny. Evol. Dev. 4, 426-34.

Owen, G., Trueman, E. R., Yonge, C. M., 1953. The ligament in the Lamellibranchia. Nature 171, 73-5.

Ronquist, F., Huelsenbeck, J. P. 2003. MRBAYES 3: Bayesian phylogenetic inference under mixed models. Bioinformatics 19:1572-1574.

Schmidt, H. A., Strimmer, K., Vingron, M., von Haeseler, A., 2002. TREE-PUZZLE: maximum likelihood phylogenetic analysis using quartets and parallel computing. Bioinformatics 18, 502-4.

Shigeno, S., Sasaki, T., Moritaki, T., Kasugai, T., Vecchione, M., Agata, K. 2008. Evolution of the cephalopod head complex by assembly of multiple molluscan body parts: Evidence from Nautilus embryonic development. J. Morphol. 269, 1-17.

Stamatakis, A. 2006. RAxML-VI-HPC: Maximum Likelihood-based Phylogenetic Analyses with Thousands of Taxa and Mixed Models., Bioinformatics 22, 2688–2690

Technau, U., 2001. Brachyury, the blastopore and the evolution of the mesoderm. Bioessays 23, 788-94.

Waller, T. R., 1998. Origin of the Molluscan Class Bivalvia and a Phylogeny of Major Groups. *In* "Bivalves: An Eon of Evolution" (P. A. Johnston and J. W. Haggart, Eds.). University of Calgary Press, Calgary.

Waller, T. R., 1990. The evolution of ligament systems in the Bivalvia. *In* "The Bivalvia - Proceedings of a Memorial Symposium in Honour of Sir Charles Maurice Yonge, Edinburgh, 1986" (B. Morton Ed.) Hong Kong University Press, Hong Kong.

Wanninger, A., Haszprunar, G., 2001. The expression of an engrailed protein during embryonic shell formation of the tusk-shell, *Antalis entalis* (Mollusca, Scaphopoda). Evol. Dev. 3, 312-21.

Wilkins, A. S., 2002. The Evolution of Developmental Pathways. Sinauer Associations, Inc., Sunderland.

Yasuo, H., Satoh, N., 1994. An ascidian homolog of the mouse *Brachyury (T)* gene is expressed exclusively in notochord cells at fate restricted stage. Dev. Growth Differ. 36, 9-18.

Yu, J. K., Satou, Y., Holland, N. D., Shin, I. T., Kohara, Y., Satoh, N., Bronner-Fraser, M., Holland, L. Z., 2007. Axial patterning in cephalochordates and the evolution of the organizer. Nature 445, 613-7.

Figure Legends

Figure 1. Brief overview of the oyster development. (A) Animal view of the 2-cell stage *S.kegaki* embryo. (B) Animal view of the 4-cell stage. (C) Animal view of the 8-cell stage. (D) Dorsal view of the 16-cell stage *Trochus* embryo [redrawn after(Dan et al., 1983)] to illustrate the typical cleavage pattern of the gastropod embryo. Note that the 2d blastomre is smaller than the sister vegetal macromere, 2D. (E) and (F): Characteristic cleavage pattern of the bivalve embryo. The blastomere X (the largest descendant of the 2d blastomere in bivalve embryos) is colored in gray. The blastomere X is the largest blastomere in bivalve embryos. (E) Lateral view of the 9-cell stage *S. kegaki* embryo. Note that the 2d micromere is the largest cell in the embryo. (F) Animal view of the 48-cell stage *S. kegaki* embryo. The blastomere X is the first cell to divide bilaterally in the bivalve embryo. (G)-(L): Morphogenesis of the bivalve embryo featuring the formation of the shell field. Orientations of the images are indicated by the xyz axes at the right side of the images. (H, J, L): Line drawings of the (G, I, K), respectively. (G, H) Lateral view of the 7hpf *S. kegaki* embryo. In this stage, gastrulation is going on, and the descendants of the blastomere X cover the dorsal surface of the embryo [indicated in gray, drawn after *Unio* gastrula (Lilie, 1895)]. (I, J) Lateral view of the 10hpf *S. kegaki* embryo. In this stage both the SFI and the blastopore are clearly visible. (K, L) Lateral view of the 14hpf *S. kegaki* embryo. In this stage the SFI has already evaginated and the shell field covers the lateral surface of the embryo. The shape of the shell field is indicated by a bold broken-line. The archenteron is represented by a thin broken-line. The hinge region is represented by a bold line and two arrows by the edge of it. bp: blastopore; hg: hinge; SFI: shell field invagination; SF: shell field. Scale bar = 20 μm.

Figure 2. Cell lineage of the oyster emryo. (A) Confocal 3D projection image of the *S. kegaki* 29-cell stage embryo, stained with rhodamine-phalloidin (magenta). (B) The same image as (A), nuclear visualization with YOYO-1 (green). Scale bar = 20 μm. (C)-(F) Embryo images traced onto paper. Some blastomeres are colored to facilitate understanding of the relationship of blastomeres between two embryos in different stages. (C) and (D) The 29-cell stage embryo seen from the animal and vegetal side, respectively. The drawing of (C) is traced from the image of (A). (E) and (F) The 48-cell stage embryo seen from the animal and vegetal side, respectively. Pb: polar body. (G) Cell cleavage tree showing the timing of cell division in each blastomere up to the 49-cell stage. Blastomeres are named following the conventional spiralian blastomere nomenclature. X: 2d or the largest descendant of the 2d blastomere. The smaller descendants of X are denoted as X^1, X^2, and so on, according to the generation when they divided. M: Bilaterally divided daughter cells of the 4d micromere.

Figure 3. Confocal images of the oyster embryogenesis, 8- through 23-cell stage. (A-F) Line drawings from the confocal 3D projection images presented in (G-L). Drawings (A)-(F) were drawn after (G)-(L), respectively in this order. (A, G) 8-cell stage, animal view. (B, H) 8-cell stage, vegetal view. (C, I) 17-cell stage, animal view. (D, J) 17-cell stage, vegetal view. (E, K) 23-cell stage, animal view. (F, L) 23-cell stage, vegetal view. Scale bar = 20 μm. The two sister blastomeres which divided from the earlier stage are indicated by bold line connecting them. X: 2d or the largest descendant blastomere of 2d. The smaller descendants of X are denoted as X^1, X^2, and so on, according to the generation when they divided.

Figure 4. Confocal images of the oyster embryogenesis 29- through 48-cell stage. (A-F) Line drawings from the confocal 3D projection images presented in (G-L). Drawings (A)-(F) were drawn from (G)-(L), respectively in this order. (A, G) 29-cell stage, animal view. (B, H) 29-cell stage, vegetal

view. (C, I) 39-cell stage, animal view. (D, J) 39-cell stage, vegetal view. (E, K) 48-cell stage, animal view. (F, L) 48-cell stage, vegetal view. Scale bar = 20 μm. The two sister blastomeres which divided from the earlier stage are indicated by bold line connecting them. X: the largest descendant of the 2d blastomere. The smaller descendants of X are denoted as X^1, X^2, and so on, according to the generation when they divided. M: 4d or the bilaterally divided daughter cells of 4d.

Figure 5. Expression pattern of the *SkBra*. Orientations of the images are indicated by the xyz axes at the right side of the images. In (A) and (C) the animal side of the embryo is marked slightly red by double-staining *Sk-β-tublin* expressed in the blastomeres of the 1q2 lineage. (A) Dorsal view of the *S. kegaki* embryo at about the 30-cell stage. *SkBra* is expressed in the 3d blastomere. (B) The line drawing of (A). *SkBra* expression is represented in green and each blastomere is labeled. (C) Dorsal view of the embryo after bilateral X division. *SkBra* is expressed in three blastomeres, identified as 3d (right), X^{12} (or $2d^{22}$, middle), and 3c (left: the focus plane for the nucleus of 3c is slightly below the focus plane of the picture. The nucleus of the X^{111} blastomere is captured in the picture and masks the 3c nucleus.). (D) The line drawing of (C). *SkBra* expression is represented in green and each blastomere is labeled. (E) Lateral view of the shell field invagination stage embryo. *SkBra* is expressed in the ventral region, which reaches from beneath the blastopore through the vegetal-most part of the embryo to the dorsal side below the SFI. (G) Dorsal view of the same stage as in (E). The dorsal domain of *SkBra* expression expands to a few cells below the SFI (arrowheads). (I) Ventral view of the same stage as in (E). The ventral domain of *SkBra* expression expands to one to two cells beneath the blastopore (asterisk). (F, H, I) The line drawing of the embryo in (E, G, I), respectively. *SkBra* expression domain is represented in green. bp: blastopore; SF: shell field; SFI: shell field invagination. Scale bar = 20 μm.

Figure 6. Expression pattern of *SkEn*. Orientations of the images are indicated by the xyz axes at the right side of the images. (A) Lateral view of the shell field invagination stage embryo. *SkEn* is expressed in the entrance region of the SFI (arrowhead). (C) Dorsal view of the shell field evagination stage (about 12 hours post fertilization [hpf]). *SkEn* is strongly expressed in the cells surrounding the evaginated shell field (SF), and is also weakly expressed in the non-border shell field cells. (E) Dorsal view of the shell field evagination stage embryo (about 12 hpf), focusing on the hinge region. Although some unspecific staining could be observed, *SkEn* is not expressed in the hinge region. (G) Dorsal view of the 18 hpf embryo in which the hinge region is stained with the sense probe of *SkEn* Cell nuclei are visualized with DAPI. Note that nonspecific staining with the sense probe of *SkEn* does not correspond to the outline of shell field cells, which are indicated in gray (only the cells which can be recognized from the picture are drawn in H). (B, D, F, H) The line drawings of the embryo in (A, C, E, G), respectively. *SkEn* expression domain is represented in red. Fainter *SkEn* expression in the non-border shell field cells is represented in pink. Nonspecific staining is represented by x in the drawings. Hinge region (hg) is represented by the dashed line in the drawings. bp: blastopore; SF: shell field; SFI: shell field invagination. Scale bar = 20 μm.

Figure 7. Expression pattern of *SkDpp*. Orientations of the images are indicated by the xyz axes at the right side of the images. (A, B) Dorsal view of the embryo after the bilateral division of X. *Sk-β-tublin* (red) marks the animal side of the embryo. Nuclei are visualized with DAPI in (B). *SkDpp* is expressed in the blastomeres, identified as $1d^{12}$ (top) and X^{112} (or $2d^{212}$, bottom). (C) Lateral view of the embryo in the course of gastrulation. The blastopore is indicated by an asterisk. *SkDpp* is expressed in the two cells that are thought to be the descendants of the two blastomeres which expressed *Skdpp* in the earlier stages. (E) Lateral view of the embryo at the shell field invagination stage (10 hours post fertilization [hpf]). *SkDpp* is expressed in the cells that are on the anterior and posterior lip of the SFI

(arrowhead). In this picture the lower cell expressing *SkDpp* is missing. (G) Dorsal view of the embryo at the same stage as in (E). *SkDpp* is expressed in both cells on the upper and lower lip of the SFI (arrowhead). (D, F, H) The line drawings of the embryo in (C, E, G), respectively. *SkDpp* expression domain is represented in yellow. (I) Lateral view of a 14 hpf stage embryo. Note that the *SkDpp*-positive cells lie on the borderline of the shell field. (J) Lateral view of an embryo at a slightly later stage than in (I). In this picture, *SkDpp*-positive cells lie on the hinge region inside the shell field. (K) Dorsal view of the embryo at the same stage as in (J). Dashed lines indicate the border of the shell field. SF: shell field; SFI: shell field invagination. Scale bar = 20 μm.

Figure 8. Effect of ZfBMP on the oyster shell morphogenesis. (A) Schematic representation of the measurements taken. (Central length (cyan) of the domain surrounded by *SkEn* expression (colored in gray), and lateral length (red) of the *SkEn* expression domain.) In all figures, the length of the bars in the graph represents the mean of the measurements in the corresponding populations and error bars represent 1 SD. P-values were obtained through Welch's two-sample *t*-test implemented in the software R. (B) Central length of the shell field. (C) Lateral length of the shell field. (D) The values of lateral length divided by central length of the shell field. Note that the ratio of lateral/central length significantly decreased in the >10nM ZfBMP4 treated embryos, indicating the change of the shape of the shell field implied in the figures (E)-(J) is statistically significant. (E and F) Dorsal view of the 80 nM ZfBMP4-treated embryo. Nuclei are stained with DAPI and visualized in (F). (H, I) Dorsal view of the control embryo reared in an environment corresponding to the 80 nM ZfBMP4 treatment. Nuclei are stained with DAPI and visualized in (I). Compared to (B), many more nuclei are visible. The shape of the shell field in the figures are indicated by the dashed line, and the central length and the lateral length of the shell field are represented by the cyan arrows and the red arrows, respectively. (G) A schematic showing the shape of the shell field (gray) of the 80 nM ZfBMP4-treated embryo. (J) A

schematic showing the shape of the shell field (gray) of the control embryo. Note that in the treated embryos lateral length of the shell field decreased, causing the bar-like shell field (G) instead of the dumbbell-like shape in the control embryos (J). Scale bar = 20 μm.

Figure 9.Schematic drawings of the developmental gene expression patterns in the oyster embryo, compared with the gene expression patterns in the gastropod, *Patella vulgata*. Orientations of the images are indicated by the xyz axes around the schematics. (A) 48-cell stage, animal view. (B) 48-cell stage, vegetal view. (C) Shell field invagination stage, dorsal view. (D) Shell field invagination stage, ventral view. (E) Shell field evagination stage, dorsal view. (F) Shell field evagination stage, ventral view. (G) Post shell field evagination stage, dorsal view. (H) Post shell field evagination stage, ventral view. (I, J) Gene expression patterns of *Brachyury*, *engrailed* and *dpp* homologues in the gastropod, *Patella vulgata*. Note that *dpp* expression pattern is remarkably different between the bivalve and the gastropod, which exhibit otherwise similar gene expression patterns. *Brachyury* expression is represented in green, *Engrailed* in red, and *Dpp* in yellow. Fainter *SkEn* expression in the non-border shell field cells is represented in pink.

Supplementary Figure 1. Variations in the cleavage order in the oyster embryo. In the line drawings, the$1b^2$ lineage blastomeres are colored in dark gray and the $1c^2$ lineage blasomeres are colored in light gray. (A, B) Line drawings from the confocal 3D projection of a 21-cell stage embryo. Drawings (A) and (B) were drawn after (E) and (F), respectively.$1b^2$ blatomere has divided to $1b^{21}$ and $1b^{22}$. The $1c^2$ blastomere has not divided yet. (A, E) Animal view. (B, F) Vegetal view. (C, D) Line drawings of the confocal 3D projection of a 20-cell stage embryo. Drawings (C) and (D) were drawn after (G) and (H), respectively. Contrary to (A) and (B), $1c^2$ blatomere has divided to $1c^{21}$ and $1c^{22}$, while the $1b^2$ blastomere has not divided yet. (C, G) Animal view. (D, H) Vegetal view.

Supplementary Figure 2. Molecular phylogenetic analyses of *SkBra*. (A) Maximum likelihood tree of several *brachyury* homologs, including *SkBra*, constructed from a 196 amino acid sequence alignment corresponding to the conserved T-domain under a JTT+G model. Bootstrap values estimated from 100 replicates are shown at the nodes of the ML tree (only bootstrap values above 50 are shown). (B) Bayesian consensus tree of the same data set as in (A). A mixed model option (with Gamma approximation of among site rate variation) was used with MrBayes 3.1.2, which selected a JTT model with 100% poseterior probability. 1,000,000 generations were sampled every 100 generations and four chains, with two independent runs. A consenus tree was produced with the burnin of 2500. Numbers above nodes represent posterior probabilities, calculated from this consensus. Sequences used are from following species (with common names and accession numbers): *Scypha raphanus* (sponge, AAU95752), *Mnemiopsis leidyi* (ctenophore, ABL68078), *Pleurobrachia pileus* (ctenophore, CAE45766), *Trichoplax adhaerens* (placozoan, CAD70269), *Nematostella vectensis* (cnidarian, AAO27886), *Tribolium castaneum* (insect, NP_001034532), *Gryllus bimaculatus* (insect, BAF34148), Drosophila melanogaster (insect, NP_524031), *Platynereis dumerilii* (annelid, CAC19335), *Patella vulgata* (mollusk, CAD12821), *Lytechinus variegatus* (sea urchin, AAL27986), *Asterina pectinifera* (sea star, BAA84938), *Saccoglossus kowalevskii* (hemichordate, ACG70186), *Ptychodera flava* (hemichordate, BAA37091), *Branchiostoma floridae* (cephalochordate, Q17134), *Ciona intestinalis* (urochordate, AAD21079), *Halocynthia roretzi* (urochordate, BAA03910), *Lampetra fluviatilis* (vertebrate, AAO61498), *Danio rerio* (vertebrate, NP_571237), *Xenopus laevis* (vertebrate, NP_001084047), *Gallus gallus* (vertebrate, AAA67365), *Mus musculus* (vertebrate, Bra: NP_033335; T-brain-1: Q64336; Tbox-4: EDL15777; Tbox-5: NP_035667)

Supplementary Figure 3. Molecular phylogenetic analyses of *SkEn*. (A) Maximum likelihood tree of several *engrailed* homologs, including *SkEn*, constructed from a 60 amino acid sequence alignment corresponding to the conserved homeodomain under a JTT+G model. Bootstrap values estimated from 100 replicates are shown at the nodes of the ML tree (only bootstrap values above 50 are shown). (B) Bayesian consensus tree of the same data set as in (A). A mixed model option (with Gamma approximation of among site rate variation) was used with MrBayes 3.1.2, which selected a JTT model with 99.9% poseterior probability. 1,000,000 generations were sampled every 100 generations and four chains, with two independent runs. A consenus tree was produced with the burnin of 2500. Numbers above nodes represent posterior probabilities, calculated from this consensus. Sequences used are from following species (with common names and accession numbers): *Achaearanea tepidariorum* (spider, BAD01489), *Caenorhabditis elegans* (nematode, P34326), *Euperipatoides kanangrensis* (onychophoran, ABY60731), *Artemia franciscana* (crustacean, CAA50279), *Tribolium castaneum* (insect, NP_001034511), *Anopheles gambiae* (insect, AAB58461), *Bombyx mori* (insect, engrailed: NP_001037550; invected: NP_001037454), *Drosophila melanogaster* (insect, engrailed: NP_725059; invected: NP_523699; deformed: P07548), *Platynereis dumerilii* (annelid, CAE46753), *Nereis virens* (annelid, ABD04655), *Pristina leidyi* (annelid, AAK64219), *Helobdella triserialis* (annelid, P23397), *Chaetopterus sp.* (annelid, AAK67707), *Haliotis asinina* (mollusk, ABC00198), *Lymnaea stagnalis* (mollusk, BAF96782), *Patella vulgata* (mollusk, AAM33142), *Patiriella exigua* (sea star, AAP74561), *Saccoglossus kowalevskii* (hemichordate, AAP79298), *Branchiostoma floridae* (cephalochordate, AAB40144), *Danio rerio* (vertebrate, engrailed 2a: NP_571119; engrailed 1a: NP_571120; engrailed 2b: NP_571115; Hox-A5a: Q9YGT6), *Xenopus laevis* (vertebrate, en-1: BAA03519; en-2: NP_001095213), *Mus musculus* (vertebrete, homeo box B5: NP_032294; en-1: NP_034263; en-2: NP_034264)

Supplementary Figure 4. Molecular phylogenetic analyses of *SkDpp*. (A) Maximum likelihood tree of several bone morphogenetic protein (BMP) homologs, including *SkDpp* and *SkBMP5-8*, constructed from a 104 amino acid sequence alignment corresponding to the conserved TGF-beta domain under a WAG+G model. Bootstrap values estimated from 100 bootstrap replicates are shown at the nodes of the ML tree (only bootstrap values above 50 are shown). (B) Bayesian consensus tree of the same data set as in (A). A mixed model option (with Gamma approximation of among site rate variation) was used with MrBayes 3.1.2, which selected a WAG model with 95.7% poseterior probability. 916,700 generations were sampled every 100 generations and four chains, with two independent runs. A consenus tree was produced with the burnin of 2500. Numbers above nodes represent posterior probabilities, calculated from this consensus. Sequences used are from following species (with common names and accession numbers) : *Nematostella vectensis* (cnidaria, BMP2/4: AAR13362; BMP5-8: ABC88372), *Acropora sp*. (cnidaria, ACI90299), *Drosophila melanogaster* (insect, dpp: AAC47552; gbb: NP_477340), *Tribolium castaneum* (insect, dpp: NP_001034540; gbb: NP_001107813), *Platynereis dumerilii* (annelid, CAJ38807), *Patella vulgata* (mollusk, AAM33143), *Pinctada fucata* (bivalve mollusk, BAD16731), *Crassostrea gigas* (bivalve mollusk, CAA10268), *Lytechinus variegatus* (sea urchin, AAD28038), *Saccoglossus kowalevskii* (hemichordate, BMP2/4: ABD97262; BMP5-8: ABD97263), *Branchiostoma floridae* (cephalochordate, AAC97488), *Lethenteron japonicum* (vertebrate, BAB68395), *Gallus gallus* (vertebrate, ADMP: NP_990153; BMP2: NP_989689; BMP4: NP_990568; BMP10: CAE46407; BMP3: NP_001029991), *Xenopus tropicalis* (vertebrate, ADMP: NP_001039157; BMP2: NP_001015963; BMP4: CAC44179), *Mus musculus* (vertebrate, GDF2: NP_062379; BMP2: NP_031579; BMP3: NP_775580; BMP4: NP_031580; BMP5: NP_031581; BMP6: NP_031582; BMP7: NP_031583; BMP8a: NP_031584; BMP8b: NP_031585; BMP9: AAD56961; BMP10: NP_033886)

Supplementary Figure 5. Results of the measurements of the embryo length in the ZfBMP4 treatments. For all ZfBMP4 concentration tested, no significant ($p<0.05$) difference was observed between control and treated embryos. This result indicates that the ZfBMP4 treatments are not toxic to the embryogenesis in general.

1

Molecular and developmental basis for bivalve shell formation

Figure1

Fig. 1

Click here to download Figure: Fig.1.pdf

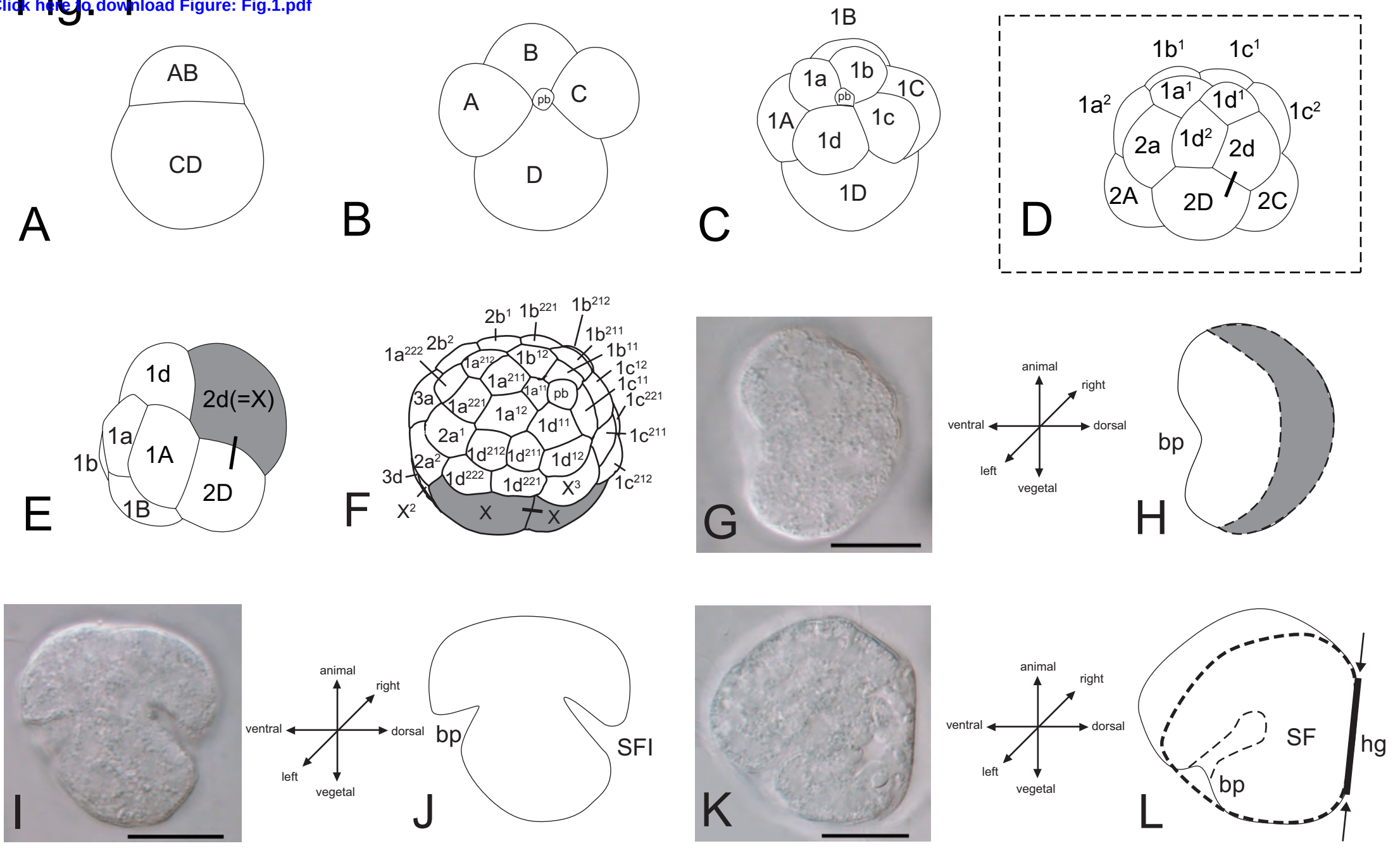

Figure2

Fig. 2

Click here to download Figure: Fig2.pdf

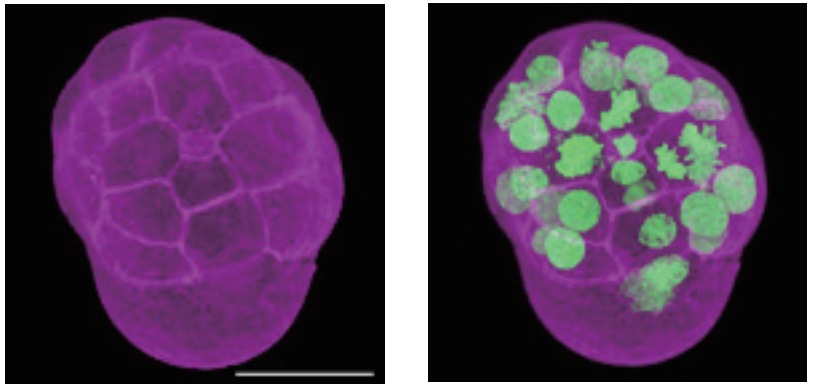

A

B

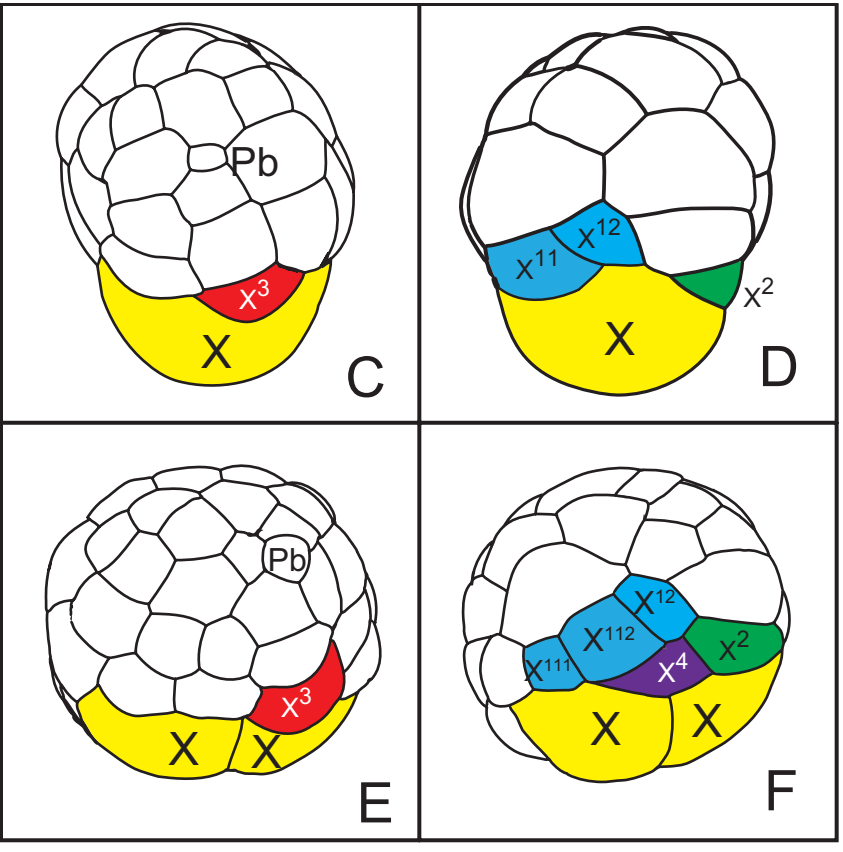

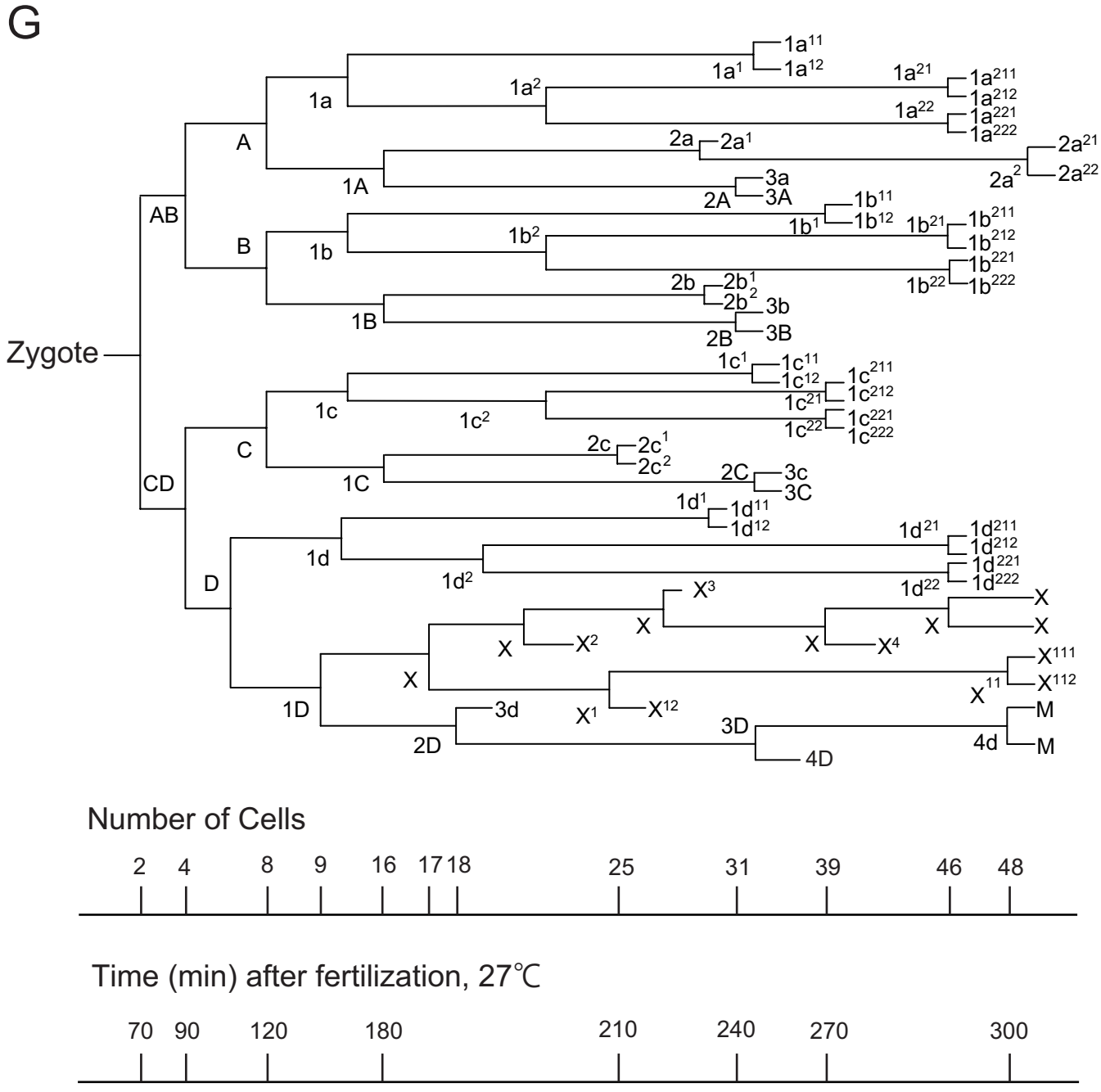

Figure3
Click here to download Figure: Fig3.pdf

Fig. 3

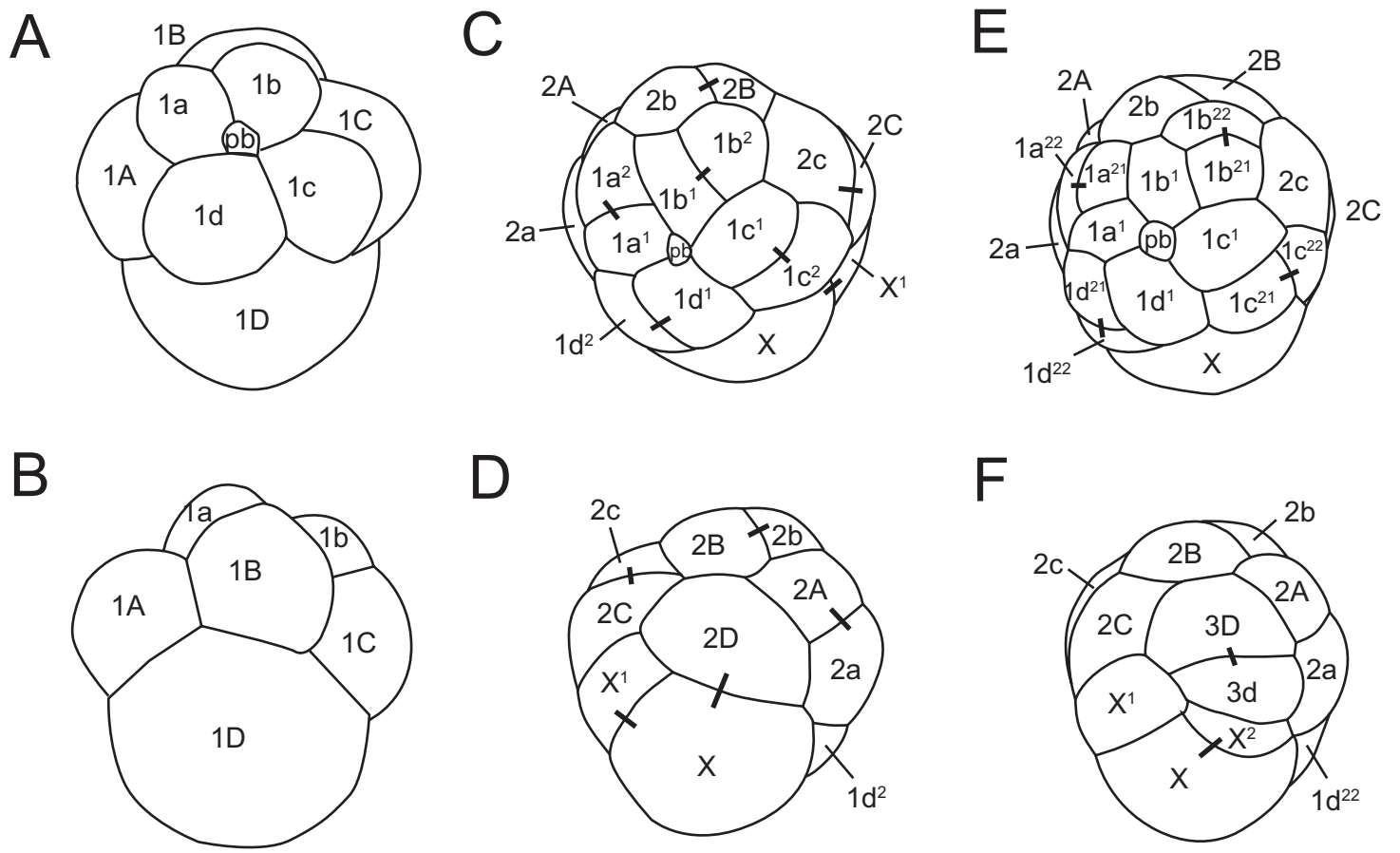

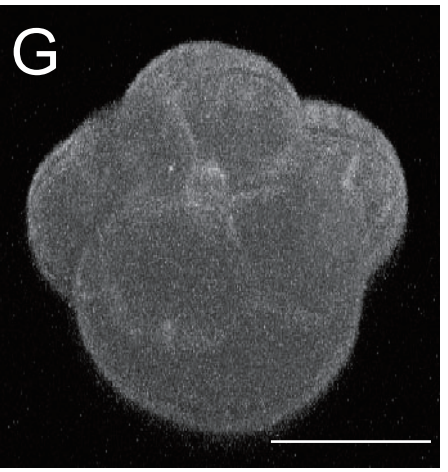

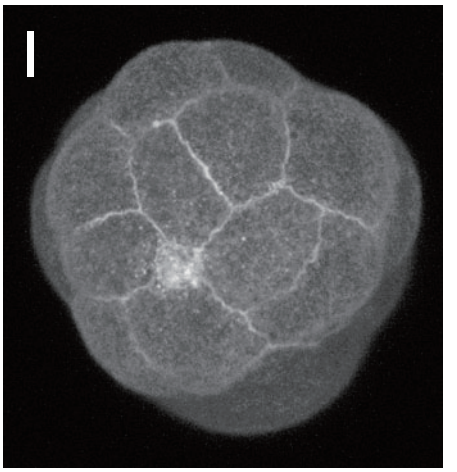

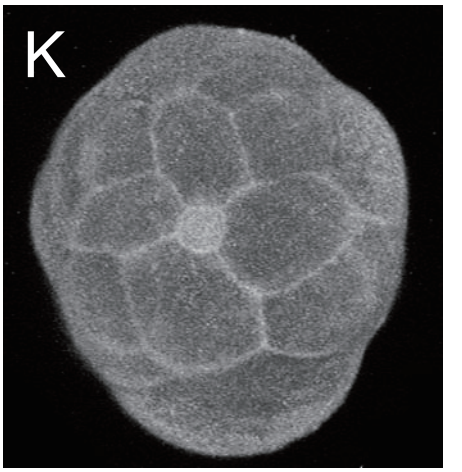

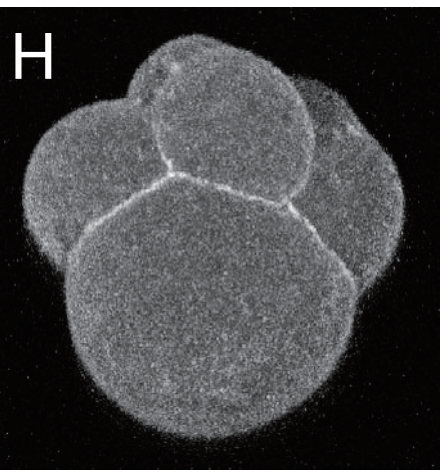

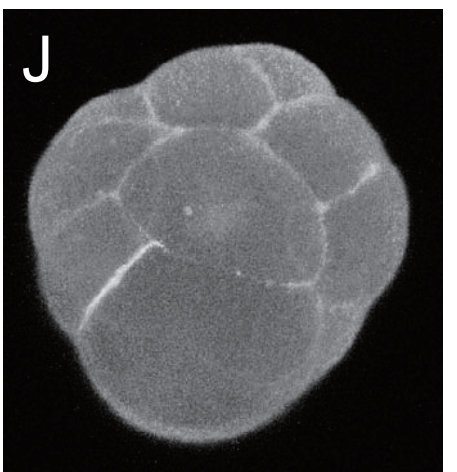

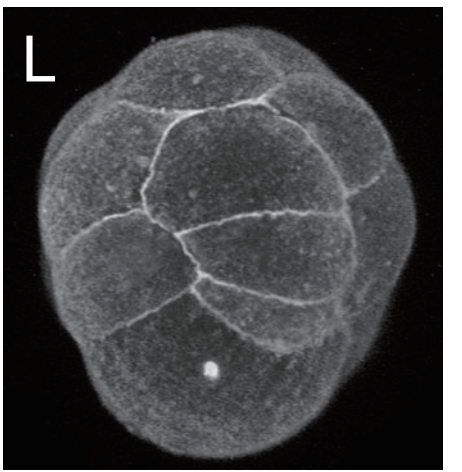

Figure4

Click here to download Figure: Fig4.pdf

Fig. 4

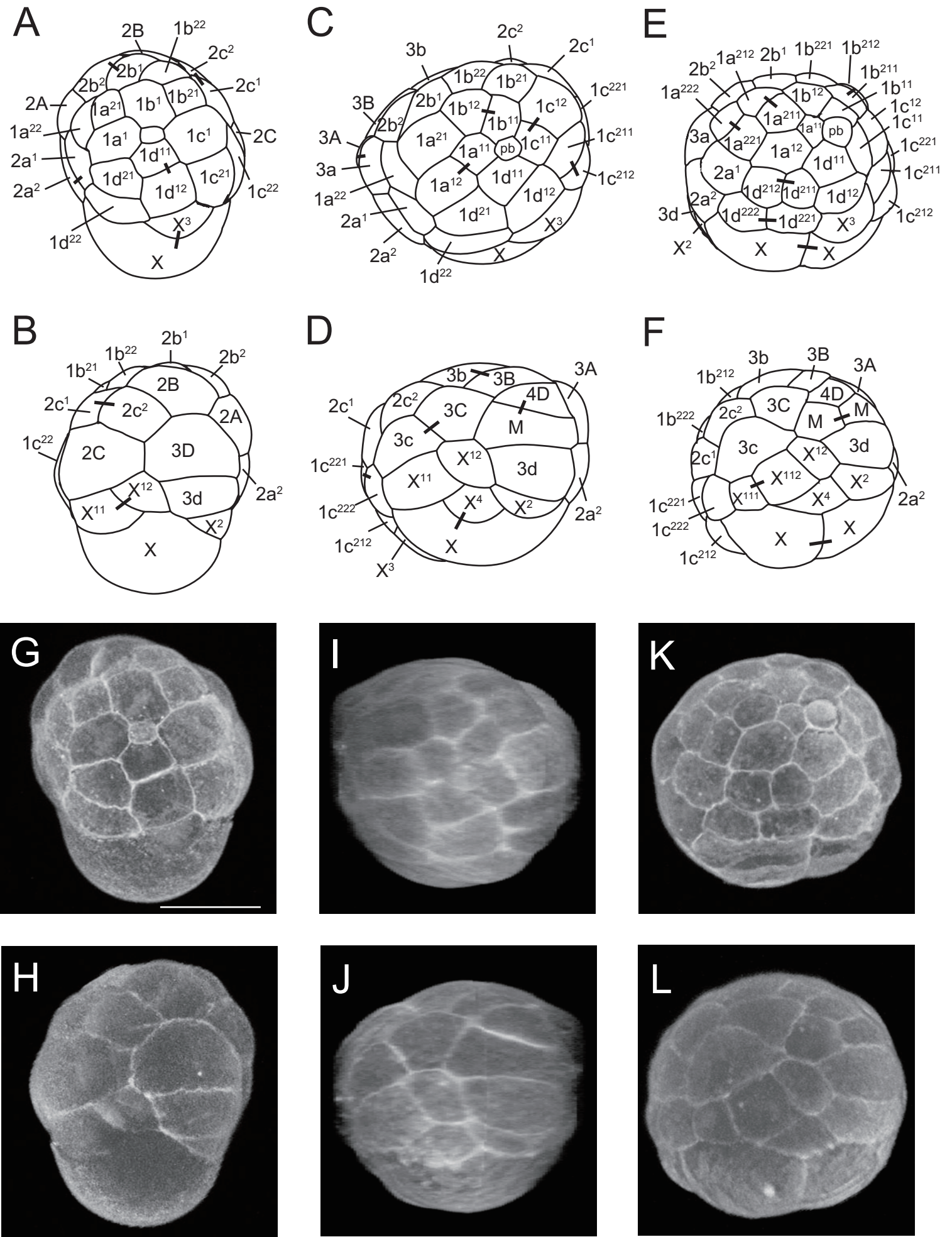

Figure5
Click here to download Figure: Fig5.eps

Fig. 5

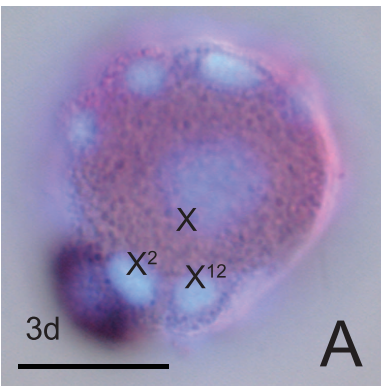

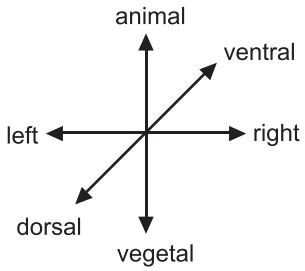

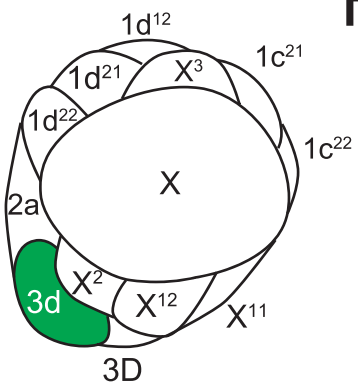

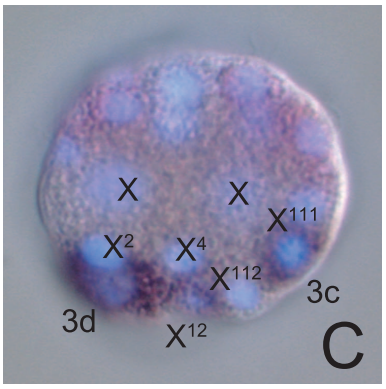

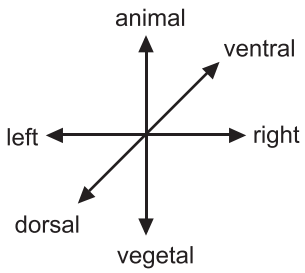

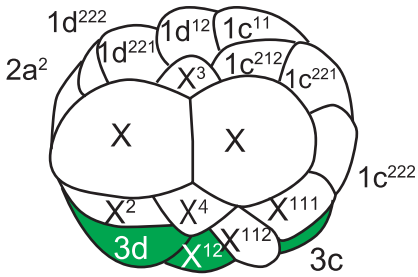

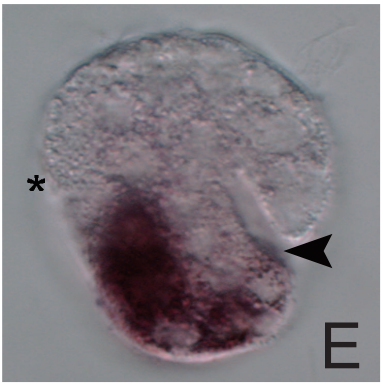

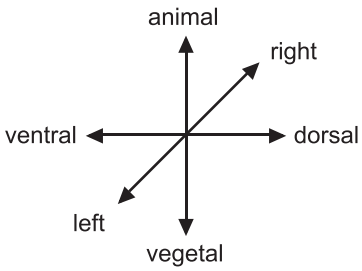

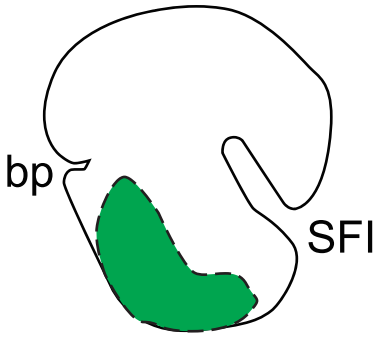

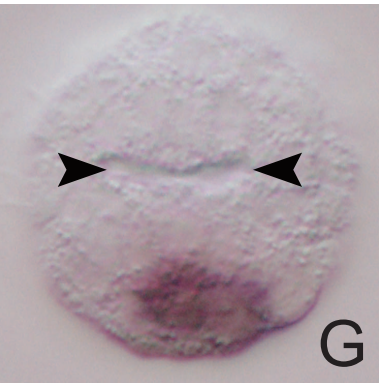

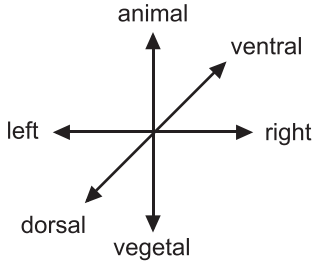

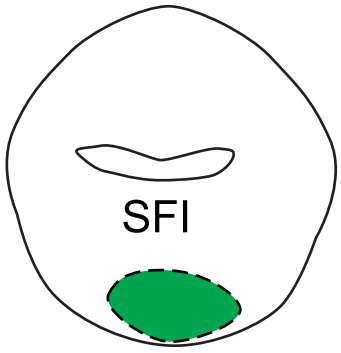

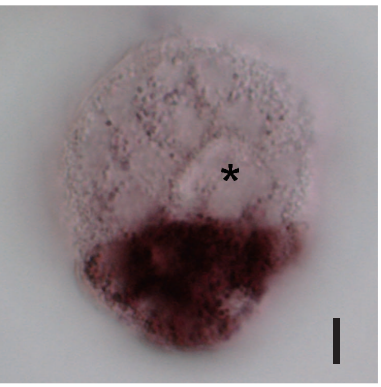

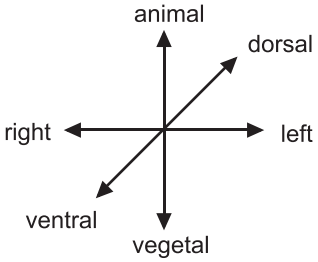

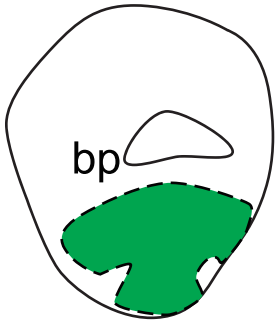

Figure6
Click here to download Figure: Fig6.pdf

Fig. 6

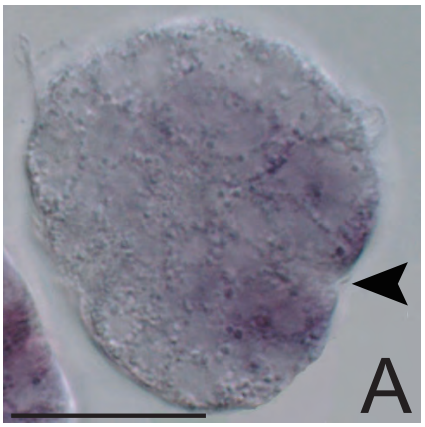

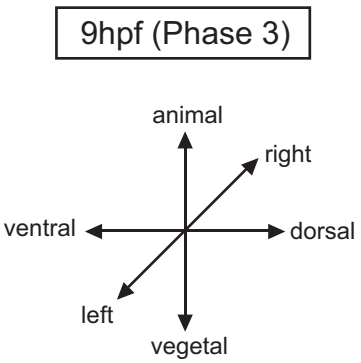

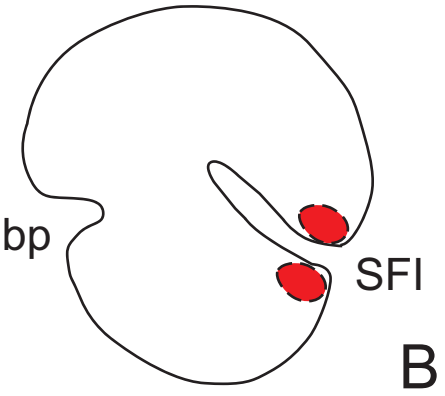

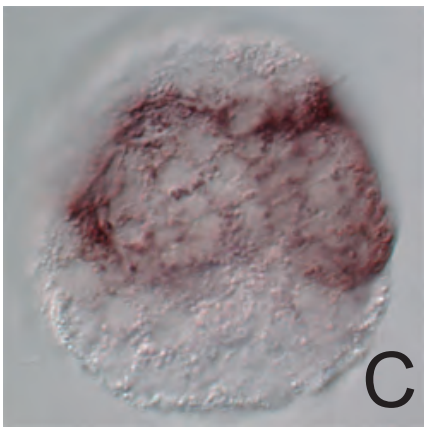

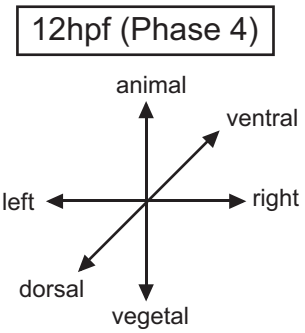

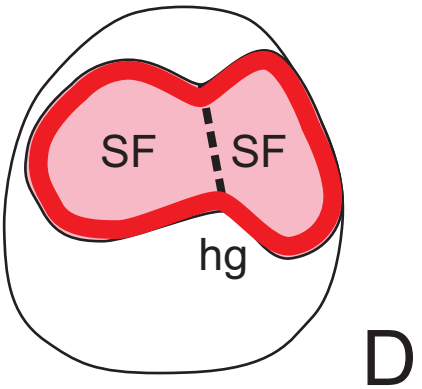

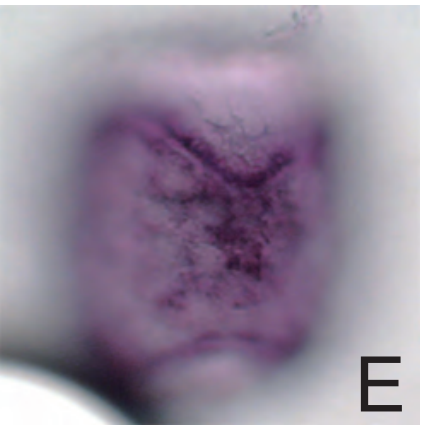

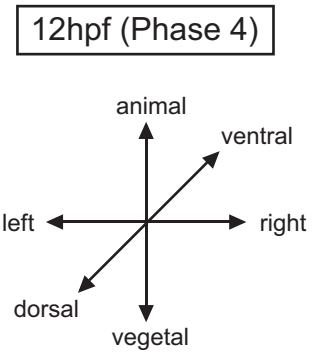

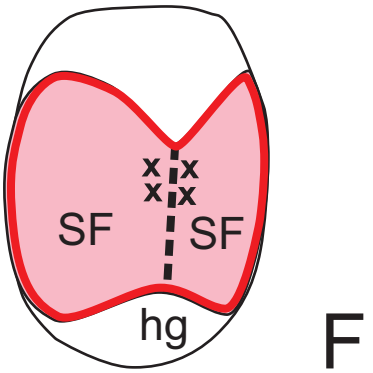

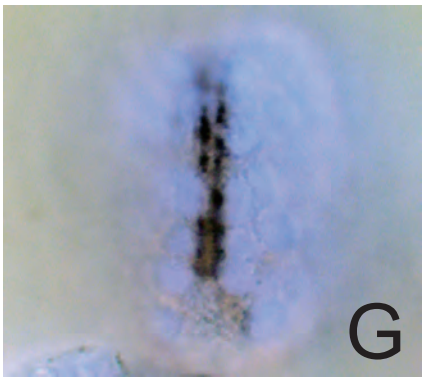

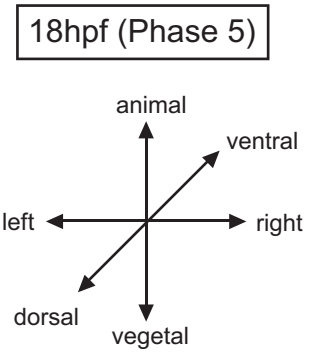

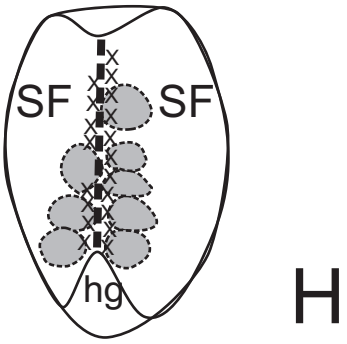

Figure7

Fig. 7

Click here to download Figure: Fig7.pdf

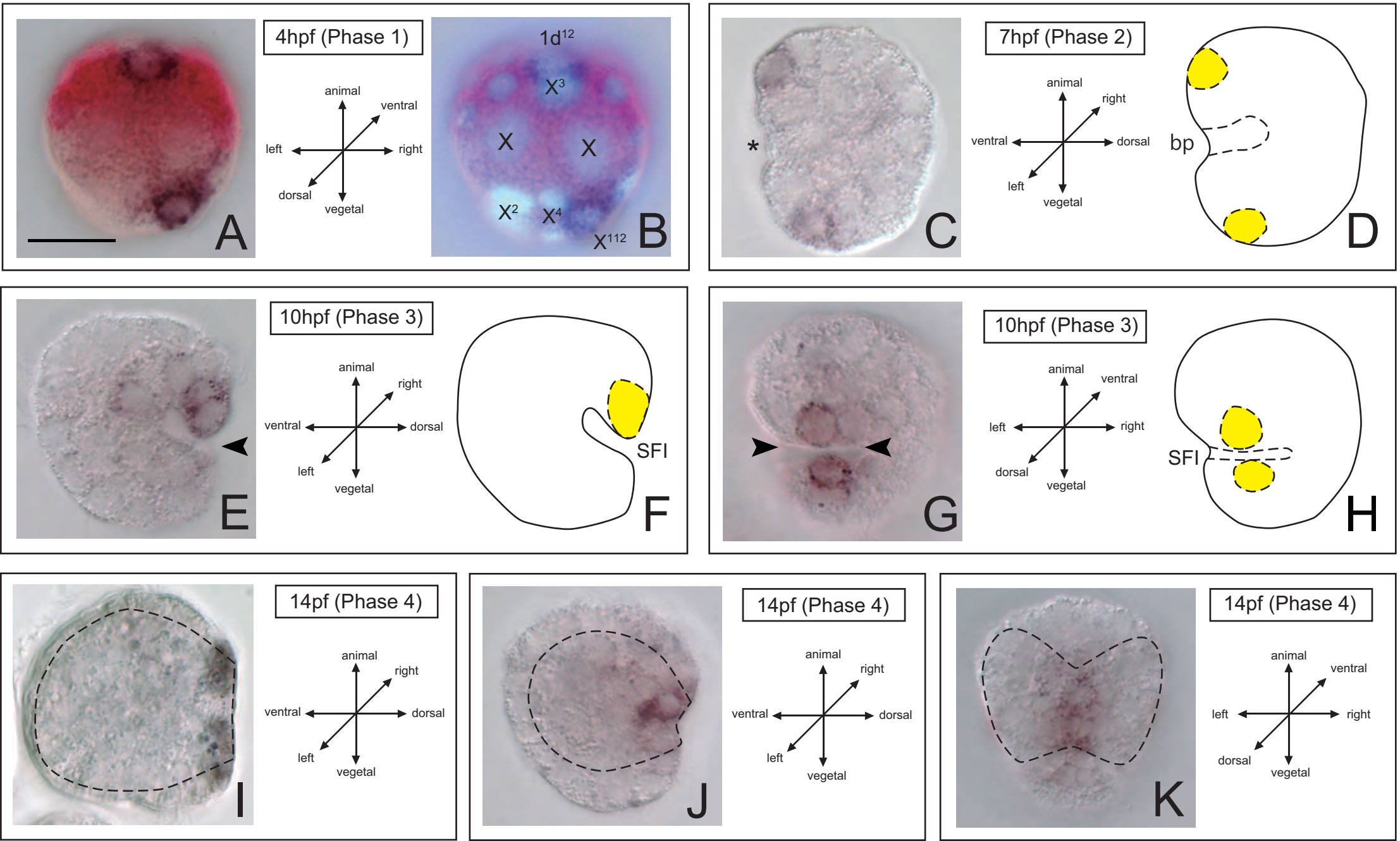

Figure8
Click here to download Figure: Fig.8.pdf

Fig. 8

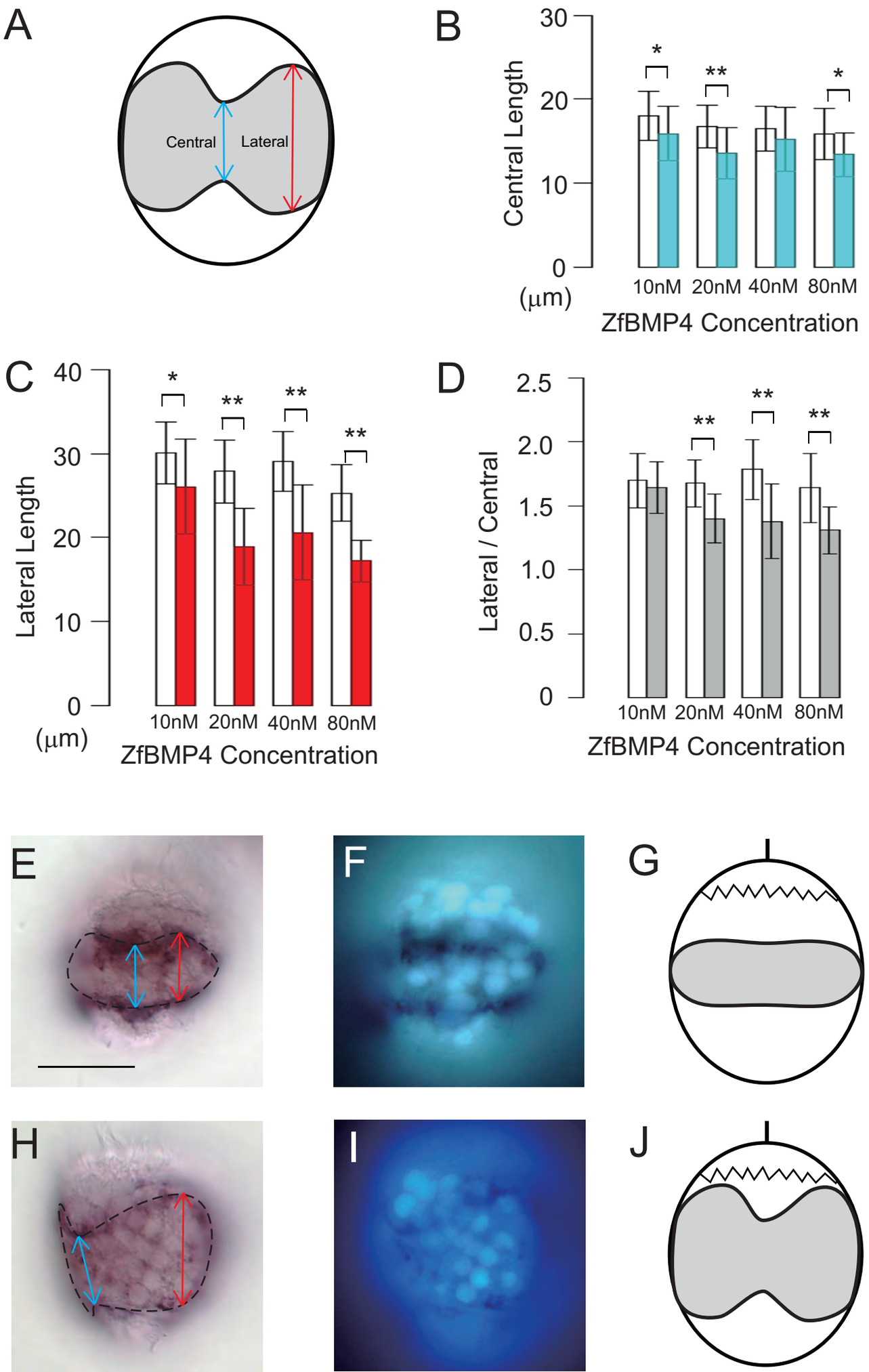

Figure9

Fig. 9

Click here to download Figure: Fig9.pdf

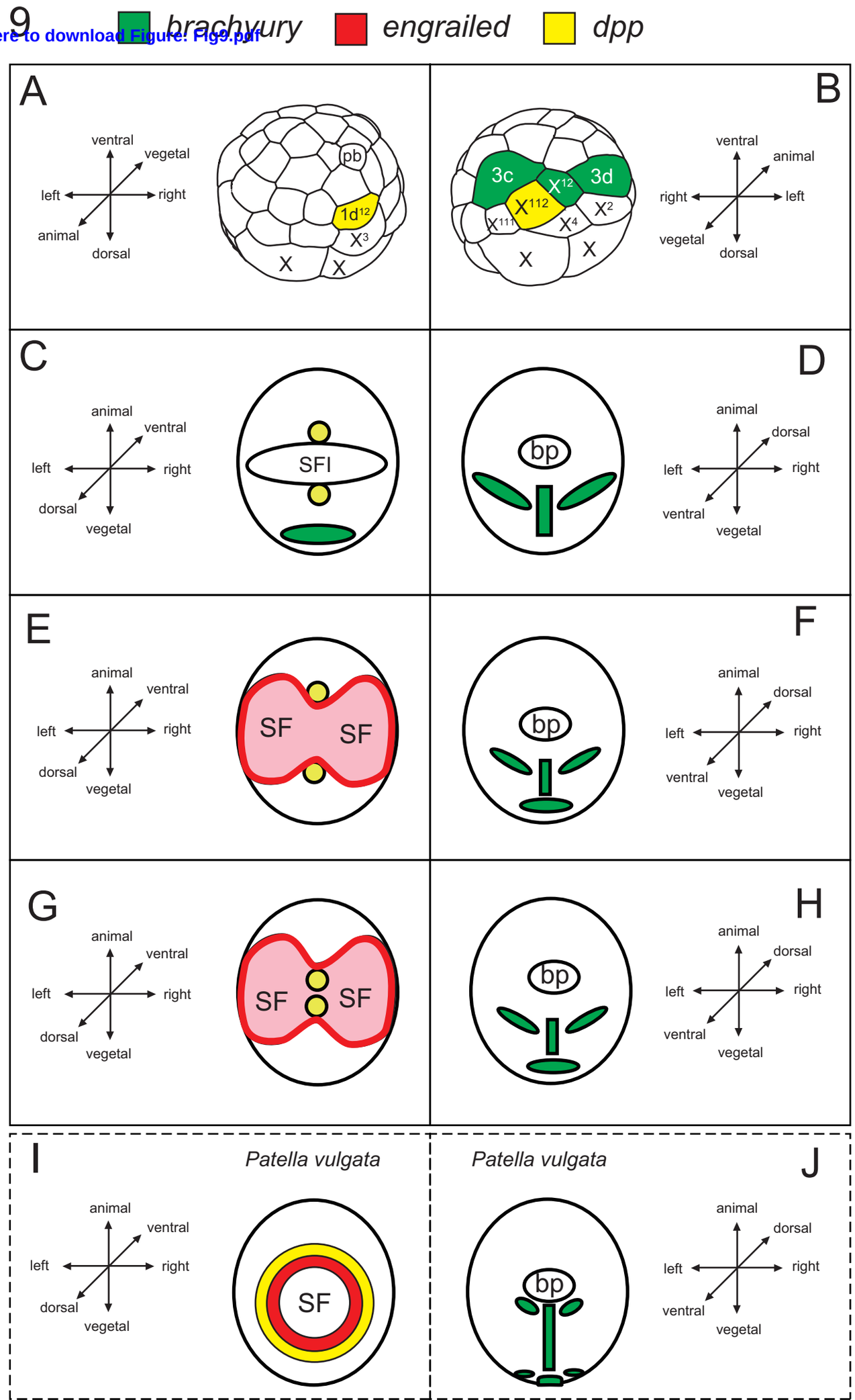

Supplementary Material

Click here to download Supplementary Material: Sup.pdf